AFRL-VS-TR-2003-1529

Space Systems Environmental Interaction Studies

M. Alvin Morgan
Alan C. Huber
David J. Sperry
Alan N. Donkin, Jr.
Scott J. Moran
Robert Redus
John A. Pantazis

AMPTEK, Inc.
6 DeAngelo Drive
Bedford, MA 01730

30 August 2001

Final Report

AIR FORCE RESEARCH LABORATORY
Space Vehicles Directorate
29 Randolph Rd
AIR FORCE MATERIEL COMMAND
Hanscom AFB, MA 01731-3010

This technical report has been reviewed and is approved for publication.

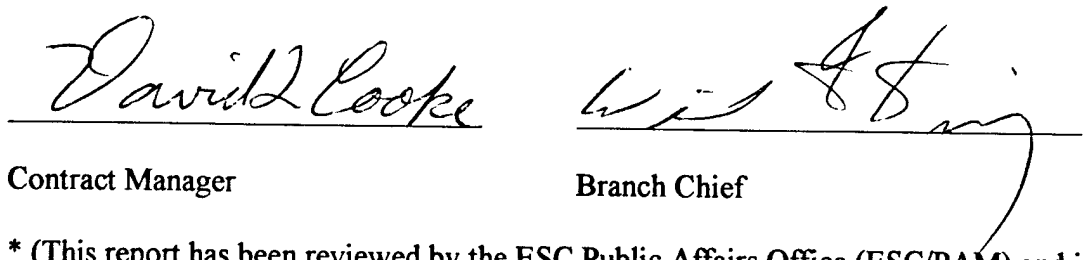

Contract Manager

Branch Chief

* (This report has been reviewed by the ESC Public Affairs Office (ESC/PAM) and is releasable to the National Technical Information Service (NTIS).)

Qualified requestors may obtain additional copies from the Defense Technical Information Center (DTIC). * (All others should apply to the NTIS.)

If your address has changed, or if you wish to be removed from the mailing list, or if the addressee is no longer employed by you, please notify AFRL/VSIM, 29 Randolph Road, Hanscom AFB, MA 01731-3010. This will help us to maintain a current mailing list.

DO NOT RETURN COPIES OF THIS REPORT unless contractual obligations or notices on a specific document require that it be returned.

* ON RESTRICTED REPORTS (CLASSIFIED/STATEMENT B) THOSE STATEMENTS IN PARENTHESIS ABOVE ARE REMOVED FROM THIS SIGNATURE PAGE

REPORT DOCUMENTATION PAGE	Form Approved OMB No. 0704-0188

1. AGENCY USE ONLY *(Leave blank)*	2. REPORT DATE	3. REPORT TYPE AND DATES COVERED
	30 August 2001	Final (August 1996 - August 2001)

4. TITLE AND SUBTITLE
Space Systems Environmental Interaction Studies

5. FUNDING NUMBERS
PE: 63410F
PR 2822 TA GC WU DD

Contract F19628-96-C-0144

6. AUTHOR(S)
M. Alvin Morgan, Alan N. Donkin Jr., John A. Pantazis, Alan C. Huber, Scott J. Moran, David J. Sperry, Robert H Redus

7. PERFORMING ORGANIZATION NAME(S) AND ADDRESS(ES)
AMPTEK, Inc.
6 DeAngelo Drive
Bedford, MA 01730-2204

8. PERFORMING ORGANIZATION REPORT NUMBER

9. SPONSORING/MONITORING AGENCY NAME(S) AND ADDRESS(ES)
Air Force Research Laboratory
29 Randolph Road
Hanscom AFB, MA 01731-3010

Contract Manager: Dr. David Cooke AFRL/VSBXR

10. SPONSORING/MONITORING AGENCY REPORT NUMBER
AFRL-VS-TR-2003-1529

11. SUPPLEMENTARY NOTES

12a. DISTRIBUTION AVAILABILITY STATEMENT
Approved for public release; Distribution unlimited

12b. DISTRIBUTION CODE

13. ABSTRACT *(Maximum 200 words)*

This report describes the objectives and summarizes the outcome, of the work performed under this contract. In addition, and this constitutes the major portion of the report, a comprehensive summary of all the important design elements for the anticipated DIDM-3 instrument is presented herein. As the final effort of the contract, all of the various facets to designing and building a Digital Ion Drift Meter for inclusion in the Communication/Navigation Outage Forecast System (C/NOFS) spacecraft's instrument suite, within the imposed size and power constraints, and capable of realizing the desired measurement performance, were looked at and analyzed. An instrument design featuring a Backgammon type anode with four charge amplifiers and four Digital Pulse Procvessors (DPP) was examined in-depth, in order to determine the following: (i) if a design can be produced which provides optimal performance, and (ii) whether the design provided adequate imaging resolution for the drift measurements. The design optimization efforts were reported on in a previous AFRL publication (AFRL-VS-TR-2001-1660). An indication of the expected measurement accuracy and resolution is included here.

14. SUBJECT TERMS	15. NUMBER OF PAGES
Digital Ion Drift Meter, DIDM-3, Communications/NAvigation Outage Forcast System, C/NOFS, Spread-F phenomena, Backgammon Anode, Pre-Amplifiers (A111), Custom MCP, Digital Pulse Processor (DPP).	33
	16. PRICE CODE

17. SECURITY CLASSIFICATION OF REPORT	18. SECURITY CLASSIFICATION OF THIS PAGE	19. SECURITY CLASSIFICATION OF ABSTRACT	20. LIMITATION OF ABSTRACT
Unclassified	Unclassified	Unclassified	SAR

TABLE OF CONTENTS

Section	Page
1. INTRODUCTION	1
2. TASK #1 – ADVANCED SPACE EXPERIMENT TECHNOLOGY DEVELOPMENT FOR THE MEASUREMENT OF BULK PLASMA PARAMETERS	1
2.1 Program Definition	1
2.2 Summary of Activities	1
3. TASK #2 - ADVANCED SPACE EXPERIMENT DATA ANALYSIS	2
3.1 Program Definition	2
3.2 Summary of Activities	2
4. TASK #3 – ADVANCED SPACE EXPERIMENT MINIATURIZATION	3
4.1 Program Definition	3
4.2 Summary of Activities	3
5. THE DIDM-3 INSTRUMENT	3
5.1 Objectives	3
5.1.1. Performance Requirements	3
5.2 Instrument Overview	4
5.2.1 Ion Distribution Image	8
5.3 DIDM-3 Changes	8
5.3.1 Overview	8
5.3.2 New Sensor Design – Anode	8
5.4 Anode Modeling	10
5.5 Anode Optimization	11
5.6 Electronic Noise	11
5.7 MCP Design	13
5.8 Digital Pulse Processor (DPP)	14
5.9 Sensor Design and Assembly	17
5.10 Anticipated Instrument Performance	18
6. HARDWARE DESIGN	19
6.1 Outline	19
6.2 Board Stack	20
6.3 Sensor Assembly	21
6.4 Sensor Design and Particle Gating	22
6.5 Power Supply Design	23
6.6 Other Sub-System Designs	24
7. SOFTWARE FUNCTIONALITY AND TELEMETRY DESIGN	24
7.1 Instrument Functionality	24
7.2 Commands	24
7.3 Telemetry Structure	26
8. CONCLUSION	27
REFERENCES	29

LIST OF FIGURES

No.		Page
1	Principle of Operation of Analog Drift Meter	5
2	Principle of Operation of Pin-Hole Camera	5
3	Cross-Section Schematic of DIDM sensor	6
4	DIDM-2 On-Orbit Sensor Response	7
5	DIDM-2 Sensor Anode Equivalent Pixel Map	7
6	Backgammon Anode Schematic	9
7	Evaluated Anode Designs (a) with zero-crossing region (b) without zero-crossing region	9
8	Segmented Micro-Channel Plate	13
9	MCP-Analog Design Verification Results	13
10	Anode Position Determination Signals Schematic	14
11	DPP Board Functional Schematic	15
12	Benchtop Charge Pre-Amp Outputs (left) and Corresponding DPP Analog Outputs (right)	16
13	(a) DIDM-2 Instrument (b) Proposed DIDM-3 (c) New Sensor Assembly Integration Method	17
14	(a) DIDM-3 Sensor Assembly (b) Aperture Assembly Module (c) Backplane Assembly Module	18
15	Preliminary Housing Outline Schematic	19
16	DIDM-3 Board Stack	20
17	Cross-Section View of DIDM-3 Sensor	20
18	Simulated Ion Trajectories inside DIDM Sensor Assembly from SIMION	21
19	(a) No-Gate Performance Summary for 0.006" Aperture (b) No-Gate Performance Summary for 0.003" Aperture	23

LIST OF TABLES

No.		Page
1	DIDM Requirements and Objectives	4
2	Preliminary Command Listings	25
3	Command Structure Details	25
4	Telemetry Data Format	26
5	Data in Telemetry Downlink	26

1. INTRODUCTION

This contract's objective was to further the understanding of near-earth environmental dynamics, by conducting both *In Situ* experimental studies, as well as, analytical and empirical studies of returned instrument data. The work was accomplished through three programs, identified as Task #'s 1, 2 and 3. A brief review of the scope of each program and a summary of the work performed during the report period follows in the next three sections. The material is presented in serial order, with Task #1 issues appearing first in Section 2. Final details on the DIDM-3 instrument design, which is the concluding work undertaken in Task #3, are presented in Sections 5 to 7, and the report concludes in Section 7.

2. TASK #1—ADVANCED SPACE EXPERIMENT TECHNOLOGY DEVELOPMENT FOR THE MEASUREMENT OF BULK PLASMA PARAMETERS.

2.1 Program Definition

The work under this task was focused on the conceptual design and engineering work needed to advance the capabilities of space instruments for the measurement of plasma parameters such as density, temperature and ion drift motion. The task objectives were two-fold, namely: (i) to develop the means to reliably measure ion densities in the range of 10^1 cm^{-3} to 10^7 cm^{-3}, by using digital rather than analog techniques, and thereby extend the existing dynamic range for such measurements by at least three orders of magnitude. (ii) to determine the incident angle of ions into the instrument within 3° in two dimensions, to allow accurate determination of ion drift velocities. The work was to build on efforts previously undertaken by Amptek, Inc. under the Digital Ion Drift Meter (DIDM) program.

There were three phases to this task. Phase 1 was essentially concerned with testing and calibrating the first DIDM-1 instrument. The effort included modifying existing mechanical and electronic designs as needed, as well as, designing and fabricating the required test support equipment (hardware and software), in order to run the instrument during environmental and system integration tests. Phase 2 dealt with the analysis of collected data during these test exercises. This was to facilitate the characterization of the instrument's performance, and the optimization of both its overall mechanical design and electronics performance. A second unit (DIDM-2) was to be fabricated, tested and calibrated in Phase 3. The tasking for Phase 3 was subsequently changed to include the fabrication and test of a third unit (DIDM-3), which was to be flown on an AFRL sponsored mission in the September 2003 timeframe.

2.2 Summary of Activities

Phases 1 and 2 of this task were concluded within the first year of the contract. The instrument was delivered to PL/GPSG (later changed to AFRL/VSBS) for calibration, and it was subsequently turned over to the space vehicle contractor (TRW Inc.) for integration onto the STEP 4 spacecraft. Details on DIDM-1 hardware, telemetry structure and software operation were reported in publications PL-TR-96-2292[1] (ADA 323403) and AFRL-VS-HA-TR-98-0029[2] (ADA 351605).

Due to a system failure on STEP 4 (the solar arrays did not deploy), no data was obtained from DIDM-1. It was not possible therefore, to make a *lessons learned* assessment of the instrument's on-orbit performance, and incorporate any change that might be deemed necessary, into the design and fabrication of the following instrument. Nevertheless, an improved capability instrument in DIDM-2 was built and successfully launched into low earth orbit on 15 June 2000 on the CHAMP spacecraft. It continues to return good data. Details on the DIDM-2 hardware development effort are reported on in publication AFRL-VS-TR-1999-1512[3] (ADA 402285). Details on early on-orbit performance, including ground support equipment data displays are provided in publication AFRL-VS-TR-2001-1660[4] (ADA 406025). As-built documentation of the

operation, commands and functions of the instrument are also available in publication AFRL-VS-TR-2001-1610[5] (ADA 323403).

The need for another instrument to follow DIDM-2 and a flight opportunity for it, were identified by AFRL even before the instrument was launched. Meetings were convened early in the year 2000, in order to discuss the requirements for DIDM-3 on the Communication/Navigation Outage Forecast System (C/NOFS) spacecraft. The essential requirement identified in the proceedings was the need to increase instrument performance by at least two orders of magnitude (a factor of 100), in the ability to make an important parameter (i.e. ion density fluctuation) measurement. It was consequently recognized that a significant instrument redesign was necessary, in order to satisfy both the mission's requirements and the spacecraft's resource constraints. Much of the time since then has been spent on the redesign effort for DIDM-3. An initial report on accomplishments in this regard was also reported in AFRL-VS-TR-2001-1660[4]. A comprehensive summary of the instrument design is provided in Section 5 of this report. It will be seen that the essential contract requirements to provide an instrument within the DIDM-2 size, weight and power constraints, yet capable of providing the information on ion density, density fluctuations (scintillation) and ion drift velocity of interest to the C/NOFS mission, has been met. In addition, because of its unique measurement technique, small size and minimal hosting requirements, another role for the instrument is clearly identified. DIDM-3 offers in a very a small package, the possibility of making good electric ($\vec{E}$) field measurements in space, without the use of the necessarily long booms of the more typically used double probe detection technique.

3. TASK #2—ADVANCED SPACE EXPERIMENT DATA ANALYSIS.

3.1 Program Definition

The work in this area was concerned with characterizing electron beam—space plasma interactions and the dynamic I-V particulars of a magnetized plasma, in order to advance the understanding of dynamic space plasma effects, through the analysis of scientific data collected by some of AFRL's advanced space plasma experiments. Efforts were directed toward the analysis of data from the Shuttle Potential REturn Experiment (SPREE) on both Tethered Satellite Systems flights (TSS-1 and TSS-1R), as well as, from the Space Wave Interactions with Space Plasmas Experiment (SWIPE) flown on the Observation of Electric-field Distributions in Ionospheric Plasma: a Unique Solution (OEDIPUS-C) mission. The analysis of data from the LAngmuir TURbulence (LATUR) rocket mission subsequently came within the scope of work for this task as well. The primary purpose for this effort was to come to grips with the interactions between rockets and spacecraft with the space environment, in order to advance the state-of-the-art capability of Air Force assets in the low-earth orbit environment.

3.2 Summary of Activities

All work on this task was concluded in the third year of the contract. A big effort was undertaken to produce a suitable analytical data display software package during the first two years. The initial version of the program was used to analyze TSS data. It was then extensively upgraded to handle OEDIPUS-C data as well. An full report on this effort was reported in publication AFRL-VS-HA-TR-98-0029. The software package was further enhanced to process LATUR flight data, following the successful launch of that rocket mission. A report on these enhancements and analysis displays from the returned data are presented in publication AFRL-VS-TR-1999-1512[3].

Throughout the time period of this effort, scientific papers were written on the data analysis findings. Some were presented at scientific conferences in the form of talks or posters, but most were published in relevant peer reviewed journals. A listing of the publications in scientific journals, resulting from work accomplished under this task appears in publication AFRL-VS-TR-2001-1660[4].

4. TASK #3—ADVANCED SPACE EXPERIMENT MINIATURIZATION.

4.1 Program Definition

The work in this area was concerned with the conceptual design and engineering work needed to reduce the size, weight, power and telemetry requirements of future advanced space plasma experiments. A principle objective was to improve the performance of particle correlator hardware, while simultaneously reducing the size, mass and power requirements. Working with the Space Science Center (SSC) at the University of Sussex in the UK, Amptek, Inc. has been at the forefront of particle correlator development in space physics applications. The first correlator to be flown in space was provided by SSC in 1980. Since then, the collaborative effort has continually improved the processing capability of the devices, by making use of the latest generation of hardware elements such as microprocessors and programmable gate arrays.

4.2 Summary of Activities

All work on this task was concluded with the successful launch of the LAngmuir TURbulence (LATUR) rocket mission, from the NASA launch range in Puerto Rico, on 11 Mar 98. Amptek, Inc. provided the Data Processing Unit (DPU) for AFRL's Energetic Particle Instrument (EPI) suite on LATUR. This DPU contained a particle correlator with an enhanced design, based on one used previously for other related missions. A detailed description of the mission specifics and DPU design is provided in publication AFRL-VS-HA-TR-98-0029[2]. Closing details on the mission and its accomplishments appear in publication AFRL-VS-TR-1999-1512[3].

5. THE DIDM-3 INSTRUMENT

5.1 Objectives

As the name implies, DIDM-3 is the third version in the DIDM instrument development effort. To date, the task has been a joint AFRL/Amptek undertaking, with the DIDM-1 and -2 sensor design, fabrication and assembly the responsibility of AFRL, as was the task of instrument calibration and performance analysis. Amptek on the other hand, designed and built the sensor anodes, electronics and instrument housing, to satisfy the physical constraints and achieve the performance requirements specified by AFRL. In DIDM-3, Amptek Inc., will provide all instrument hardware, and carryout most of the performance analysis necessary to optimize instrument performance. AFRL will remain responsible for the GSE and data analysis software. The essential contract requirement here is to provide an instrument with the same functionality as DIDM-2, but capable of meeting the more stringent drift measurement requirements of the C/NOFS mission. The ultimate objective is to establish the small, light weight and low power DIDM package as a means of making good electric ($\overline{E}$) field determinations in space. The C/NOFS mission provides the unique opportunity for direct comparison of ion density, ion temperature and $\overline{E}$ field measurements from different instrument platforms.

5.1.1 Performance Requirements

The requirements for DIDM-3 are summarized in Table 1. In a bid to make the instrument suitable for additional missions, the environmental objectives were derived from three sources, namely the NPOESS, C/NOFS, and TechSat program specifications. NPOESS lists both "specification" and "objective" levels, where the objective level is more stringent. For NPOESS, it is necessary to meet the specification level and desirable to meet the objective level as well. Each of these sources constitutes a challenging set of requirements and combining them does not make the task any easier. However, meeting these AFRL specified requirements potentially ensures that the instrument is considered for all three missions.

Table 1. DIDM Requirements and Objectives

		NPOESS Specification	NPOESS Objective	C/NOFS Objective	TechSat Objective
Drift Velocity	Range (km/sec)	0 to 3	0 to 5		
	Precision (m/sec)	50	25	10	
	Accuracy (m/sec)	75	50	10	
Plasma Density	Range (cm^{-3})	$5x10^3$ - $5x10^6$	10^2-10^7		
	Accuracy	20%	5%	1%	
	Resolution (km)	50	10	1	0.01
Plasma Temperature	Range (K)	500 to 10,000			
	Accuracy	10%	5%		
	Resolution (km)	100	10 km		
Plasma Fluctuations	Resolution (km)	100	10		0.01
	ΔN/N	10^{-2} to 1	10^{-4} to 1		
	Precision of ΔN/N	Greater of 20% or 10^4 cm^{-3}	5% or $2x10^2$ cm^{-3}		

A resolution for the drift measurement is not listed explicitly in Table 1. NPOESS does not appear to specify a spatial resolution for this measurement. It is known that AFRL theorists desire a spatial resolution of 3.5 meters for C/NOFS, but the Principal Investigator (PI) has indicated that a reasonable objective would be 200 m with a precision of 25 m/sec, and the capability to measure the drift more frequently with an attendant loss of precision. Note that in some requirements both precision and accuracy are separately called out, while in other requirements only one is given. It is understood that precision refers to random fluctuations in repeated, identical measurements while accuracy refers to errors due to systematic effects. Where these are not separately specified, it is assumed that the total combination of the two is the intended quantity. It is also assumed that these quantities are all specified in terms of "rms" rather than "FWHM"

5.2 Instrument Overview

The goal of DIDM is to measure the ion temperature, ion density, and all three components of the ion drift velocity (note that since $\vec{E} = \vec{v} \times \vec{B}$, a drift velocity measurement and a magnetic field measurement also yields an electric field measurement without the use of long booms). In the past, the five quantities of the ion plasma population were measured using two instruments, a Retarding Potential Analyzer (RPA) and a Drift Meter. A typical RPA consists of a small enclosure with an aperture through which incident particles (ions and electrons) enter, grids in the aperture to which an electric potential is applied to selectively retard incident particles, and a collector with attendant electronics to measure the transmitted flux. The total number through the aperture, with zero retarding potential and a negative potential on the collector, yields the ion density. In order to determine temperature and the component of drift velocity parallel to the spacecraft velocity vector, the retarding potential is varied and the flux vs. potential measured. In the simplest case, a zero temperature single component plasma, the flux would vanish when the retarding potential reached the kinetic energy associated with the parallel velocity. In the real case, with non-zero temperature, the temperature determines the range of energies over which the flux vanishes. The presence of a mixed

ion population complicates the flux vs. voltage relationship, but the individual components can be successfully recovered by the application of appropriate data-processing techniques.

Virtually all previous space plasma drift meter instruments of the so-called Analog Drift Meter (or ADM) type, make use of relatively large apertures (equivalent to low f-number optics) and a segmented anode, typically four flat conducting plates, mounted behind a wire grid and facing into the spacecraft's ram direction[6] (see illustration in Figure 1). These instruments measure the total current into the four plates using analog electronics circuitry, as a function of the applied grid voltage. In the RPA fashion, the grid voltage in an ADM sensor is typically varied from 0V to between +20V and +30V. The shape of the ion current-voltage curve is a function of the ion density, temperature, composition, and parallel drift velocity. By measuring the relative currents into the four quadrants, the centroid of the drift is determined, and from this, the perpendicular drift velocity.

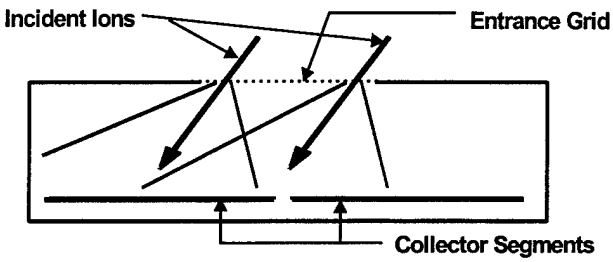

Figure 1:
Principle of Operation of Analog Drift Meter

This type of instrumentation works well as long as the ambient plasma density is in the range of 10^3-10^6 cm^{-3}. When the density drops below the 10^3 cm^{-3} level, the ion current is reduced to the magnitude of the inherent electronics noise and becomes too small to be reliably measured. These instruments are inherently limited by the electronic noise of the current measurement. Since they measure the net current, when the plasma density is too low, no measurement is possible. Furthermore, these instruments are typically not solar blind, so that the generation of secondary electrons from the collector surface seriously compromises the instrument's performance, if it is facing in the direction of the sun. This often imposes a significant constraint on the operational use of the device.

The large aperture provides measurable current and makes it possible to ignore the thermal effects of heavy ions such as O^+. The effect of light ions however (in the so-called 'thermal signature') can sometimes complicate the desired measurements. The use of only the four quadrants for imaging makes it impossible to separate the effects of the different ion mass. Additionally, it becomes difficult to determine the centroid accurately when it is far from the boundary between quadrants, and even more difficult in the presence of high temperature ions.

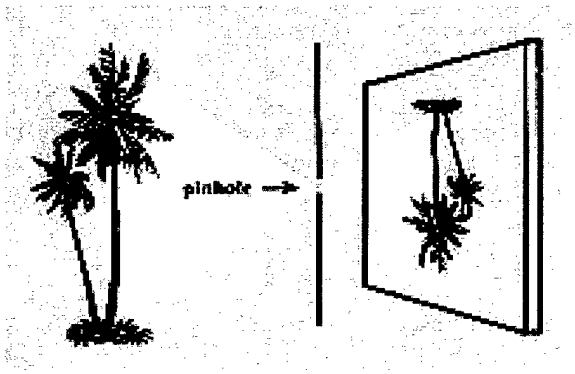

Figure 2:
Principle of Operation of Pin-Hole Camera

The Digital Ion Drift Meter, is similar to the previous instruments in that it incorporates an aperture, retarding grids and images ions. However, instead of measuring net currents, DIDM measures each individual ion. The driftmeter feature of DIDM works by imaging the ion distribution in a manner analogous to the operation of a pinhole camera (see Figure 2). With a small aperture, the position at which an ion strikes the position-sensitive anode is determined by its velocity vector, the incident angle. If the parallel velocity of the ion distribution is known from an RPA, then by measuring the two-dimensional distribution on the anode, the two components of drift velocity perpendicular to the spacecraft velocity vector are derived. The centroid of the image is associated with the mean drift, while the spreading of the image is due to thermal effects and is also related to composition, since light ions drift more.

Both the RPA and driftmeter functionality are combined in DIDM, and a position sensitive collector (anode) is used to detect incident ions.

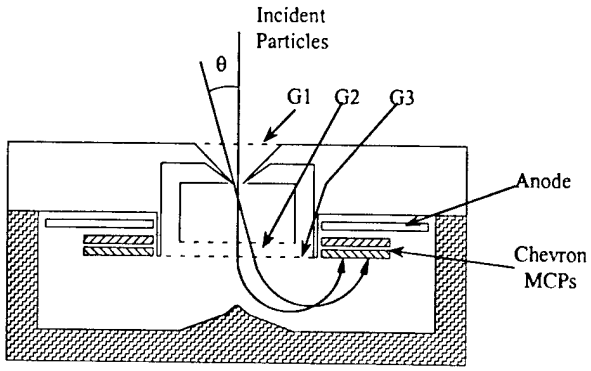

Figure 3:
Cross-section Schematic of DIDM Sensor

In RPA mode, DIDM measures the count rate versus voltage. In driftmeter mode, DIDM measures the incident position on the anode of each individual ion. The instrument offers three principal advantages over any other comparable design to date. The primary advantage is that there is no minimum density below which the instrument fails to operate. It will count ions even at the lowest density, although the instrument will require a longer time period at low densities to obtain a statistically significant result. Meaningful data at all density levels can be readily obtained. A secondary advantage is that the effects of heavy and light ions in the perpendicular drift measurement can be readily separated, due to the fact that a complete image of the ions distribution is obtained, instead of simply having the relative currents in four quadrants. The third advantage is that DIDM is solar blind, and consequently is not limited in viewing angle with respect to the sun.

Figure 3 shows a cross-sectional view of a DIDM sensor. It illustrates the measurement principle of the instrument and shows how it overcomes the solar blindness limitation. The key component which sets DIDM apart from a regular ADM is the Micro-Channel Plate (MCP). Every ion that interacts with the MCP produces a pulse which is large enough for the electronics to count. The position-sensitive anode measures the location of each output. MCPs are optically sensitive, so to achieve the necessary solar blindness ion optics is used to bend the ion trajectories as illustrated. Incident ions traverse a low transmission grid G1 (actually a series of three screens) and enter the the RPA or energy analysis region through the instrument aperture. The G1 potential is adjustable and can be used to gate the ions, to either allow or prevent them from reaching the aperture. Grid G2 may be used to apply a retarding potential (ϕ_{ret}), which is also variable. All ions with $E > \phi_{ret}$ pass through grid G2, and then through grid G3, which is held at ground potential and used to shape the electric fields inside this deflection cavity of the instrument. The electric field ensures that the ions get to the MCP detectors and that the trajectory depends only on the incident angle. The position of interaction is very nearly independent of the total energy of the ion, depending only on the incident angle.

The front surface of the first MCP is held at a nominal -2,000V, while the surrounding walls of the cavity, including the sharp point facing the entrance aperture, are held at ground potential. An electric field is thus produced, which forces incident ions to reverse direction, accelerate in the presence of the 2keV field and strike the front MCP plate. The "pointed" part of the center portion of the bottom half of the housing serves to shape the electric field lines and greatly determine the ion trajectory inside the sensor. It is also part of a backplane assembly which acts as a "light dump" to incident photons. Any sunlight (photons) that might come through the aperture is thus absorbed and prevented from getting to the MCPs to directly affect its measurement performance. Incident and/or secondarily generated electrons in the region are repulsed by the MCP potential, and are removed from the system when they strike the cavity walls. An entirely ion-induced electron charge cloud is thus generated within the MCP and collected on the backside by the position-sensitive anode, every time an ion enters the aperture of one of the two instrument sensors.

There are two basic modes of operation for DIDM. In what is often referred to as the RPA mode of operation, the grid potential on G2 is swept from 0V to some maximum voltage on the order of about +30V, and the incident ions are be counted as a function of the voltage. The data obtained in

this fashion is used to extract ion density (n_i), ion temperature (T_i) ion composition, and parallel velocity information, as discussed before. This is similar to a conventional RPA, except that by counting individual ions instead of measuring net current, lower densities can be measured. A second mode of operation, the so-called drift meter (DM) mode, is used to measure incident ion trajectories, and by extension, ion drift velocity. In this mode, the G2 voltage is set to zero to allow all ions to enter the deflection cavity. If the drift velocity is zero then all ions impinge on the entrance aperture at near normal incidence, modified only by their thermal motion. For O^+ ions for example, a thermal velocity of about 1.4 km/sec is superimposed on the approximately 7.5 km/sec orbital velocity of a typical low earth orbiting spacecraft, so that the zenith angle deviation from normal incidence is less than 10°. The azimuthal angle (rotation about the axis of cylindrical symmetry) on the other hand is arbitrary (0-360°), and a sensor will image the ions as a ring on the MCP-Anode detector. The radius of this ring will be related to the incident ion energy and its width will correspond to dispersion or spread in the zenith angle. Thus an image pattern is a distinct function of the drift velocity. A non-zero drift velocity results in the ions entering the aperture at a fixed azimuth and zenith angle (with a slight spread due to thermal motion). In this case, the ions are imaged to spot on the MCP, with the radial distance of the image spot from the central MCP hole a measure of the zenith angle, while the angular location of the spot defines the azimuth angle. Once these two angles are known, the drift velocity components can be computed.

It must be kept in mind that DIDM is a particle-counting instrument and is therefore subject to statistical error limitations in its measurements. The instrument must detect a threshold number of ions per acquisition period, in order to attain a specific level of measurement accuracy and precision. Consequently, it is not possible to achieve constant precision and accuracy over the full dynamic range of measurements. An analog sensor has a minimum density. At lower densities, the electronic noise in the current measurement obscures the current so no meaningful measurement can be made. DIDM has no such minimum density limitation since it will count ions individually, but at low densities a longer measurement time is needed to reach a specific precision. Also, at high densities incident events will overlap in the fixed period required for detection processing, effectively limiting the maximum density at which DIDM can accurately operate.

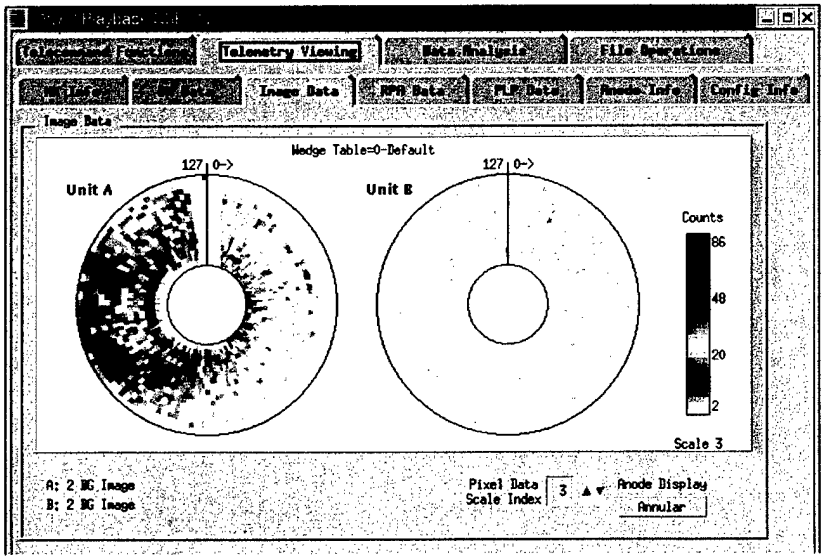

Figure 4: DIDM-2 On-Orbit Sensor Response

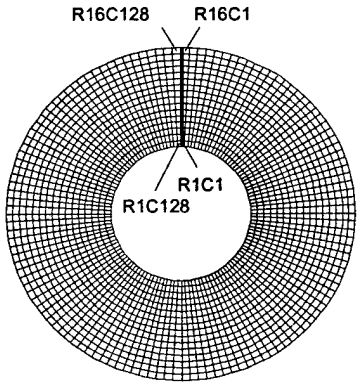

Figure 5: DIDM-2 Sensor Anode Equivalent Pixel Map

5.2.1 Ion Distribution Image

The basic approach of using a MCP and ion optics to produce a digital RPA and Drift Meter, was proven in DIDM-2. A view of the early on-orbit data returned by DIDM-2 is shown in the GSE sensor response plot for one of the two sensor heads (*Unit A*), in Figure 4. Each of the two DIDM-2 sensors resolves a 35° half-angle cone of input space onto a 16 x 128 (elevation x azimuth) pixel array at a rate up to 16Hz. An equivalent pixel map is shown in Figure 5. In order to achieve the specified performance, the DIDM-3 pixel space will be somewhat smaller, an 8 x 32 (elevation x azimuth) pixel array, but the instrument will acquire images at the substantially greater rate of up to 128 Hz, simultaneous with RPA discrimination. The heritage feature of independent control for each of the two sensor heads will be maintained.

In Figure 4, the centroid of the ion distribution is clearly visible, as is the spreading due to thermal velocity and to ion composition. DIDM-2 clearly showed that this type of sensor can image the ion population and that the ion parameters can be accurately determined[7].

5.3 DIDM-3 Changes

5.3.1 Overview

DIDM-2 demonstrated that the basic approach is viable. However, based on the experience gained in building DIDM-1 and -2, in analyzing the data, and in looking at the operational requirements of Table 1, it was clear that several improvements are needed. DIDM-3 will implement the same basic functionality as DIDM-2 but is enhanced to address these limitations. There are two major goals that drive the new design: (i) improved manufacturability and reliability and (ii) ability to measure a wider range of ambient densities.

To enhance manufacturability, DIDM-3 incorporates the sensors into the instrument, instead of using separate modules attached to the front. The interconnection beween the modules and the instrument in DIDM-2 made assembly difficult (therefore expensive) and degraded reliability. In addition, DIDM-3 employs a new anode sensor design. The DIDM-2 anode geometry required extremely tight tolerances, which resulted in difficult to make parts and high custom fabrication costs. DIDM-3 uses an anode design which can be fabricated using more conventional techniques, at lower cost and higher reliability. The new anode offers other performance advantages as well, which will be discussed later.

In order to measure a wider range of ambient densities, DIDM-3 uses much improved electronics. The circuitry is much faster (thus reducing the detect processing time) and includes several new features. In addition, new long-life MCPs are proposed for the design, so that long period operations at high count rates can be adequately accommodated.

5.3.2 New Sensor Design - Anode

A key change for DIDM-3 is in the design of the position-sensitive anode, from which the incident angle of detected particles is determined. The design adopted is the so-called *Backgammon* anode pattern, so-called because of its apparent similarity in layout to the board game of the same name, and it replaces the previous *wedge & strip* design. The pattern is illustrated in Figure 6. The circle shown represents an electron cloud impinging on the triangular shaped anode elements. These in-turn, are connected to four charge amplifiers in the manner shown, from which incident position may be determined from their outputs in two dimensions as indicated in the formulation. The design does require the use of four charge amplifiers, rather than the three per sensor needed in the current DIDM design, but this is a relatively minor drawback. There are several advantages and other important reasons for this adoption of the new design.

The first of these was the need to make the anode easier to manufacture. For various reasons, the wedge & strip design proved fiendishly difficult to make. The pattern is intricate and made-up of features that are as small as 5μm (0.0002") wide throughout. This puts a severe limitation on the number of facilities willing and capable of making the devices successfully, in the small quantities required, at an affordable price. The *Backgammon* anode pattern is much simpler in design and has feature sizes one order of magnitude larger at 25μm (0.001"). The expectation is that it will prove considerably easier (and correspondingly cheaper) to manufacture.

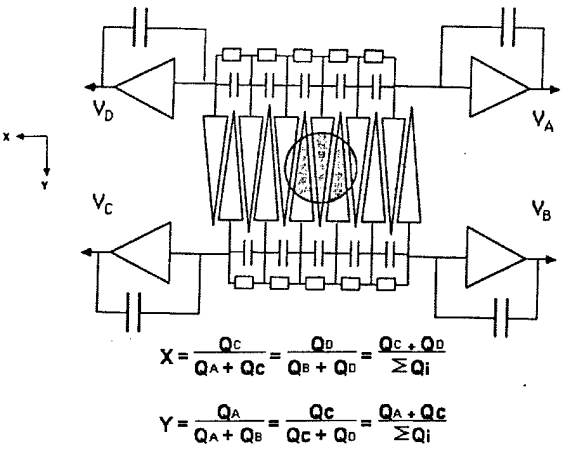

Figure 6:
Backgammon Anode Schematic

A second major reason for change has to do with the fact that the circular geometry of the sensor assembly naturally leads to the need to distinguish between 0° and 360° in incident azimuthal angle. The solution thus far has been to physically incorporate a so-called *zero-crossing mask* in the anode assembly, so as to clearly demarcate a zero-crossing boundary. However, this technique precluded particle detection in the areal extent of the mask, and for DIDM-2 approximately 15° of detection space was excluded. Various design studies were conducted in an attempt to reduce this extent. One of the virtues of the *Backgammon* design is that a distinct zero-crossing demarcation can be avoided entirely. To accomplish this, the azimuthal angle is determined from a combination of anode response and noting which half of a segmented MCP is triggered. Simulation analysis shows that the DIDM-3 anode design should easily realize better than 1% position accuracy over the full 360° extent of incident angle space.

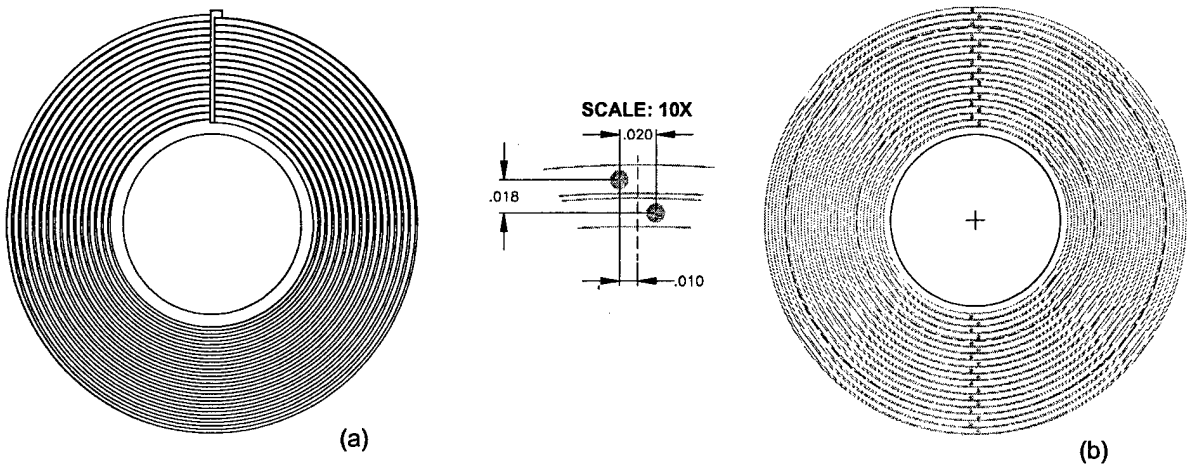

Figure 7: Evaluated Anode Designs
(a) with zero-crossing region
(b) without zero-crossing region

5.4 Anode Modeling

It was important to have some idea of the inherent "anode resolution" for the *Backgammon* design, before it was adopted. The essential question was: given ideal noise-free electronics, what would be the resolution obtained from the anode? To provide an answer, a MathCad model was created, in which the charge deposited on all the wedges in the design (30 total) was computed for a gaussian charge distribution. In reality, the DIDM anode geometry is cylindrical in shape, thus the rectangular geometry shown in Figure 6 maps into polar geometry. The wedges were modeled using analytical expressions for $\rho(\phi)$ to define the wedges, where ρ and ϕ represent radius and angle respectively, in cylindrical coordinates. It was assumed that: (1) a 1 mil tail, (2) a 15 mil head, and (3) 1 mil separations throughout. The charge distribution was modeled as a gaussian, with a σ of 10, 15, and 20 mils. MathCad computed the numerical integrals of the gaussian charge distribution between the radial and angular limits defined by the wedges. A random number generator was used to select incident locations uniformly distributed over the anode. Some important results were as follows:

1. There exists a systematic distortion: the measured elevation depends on azimuth, with a change of 1 mil over the full 360°.
    1.1. This distortion is due to the 1 mil separation between each pair of wedges: the measurement of (X1+X2)-(X3+X4) compares the position of the spot to the average of the two, and since X1 and X2 are offset from X3 and X4 by the 1 mil separation, the apparent location moves by 1 mil. If you fix a charge cloud centroid at a radial position in the middle of a wedge pair and change azimuth by 360°, then the apparent radial position varies between $\pm$0.5 mil.
    1.2. Assuming that we use about 200 mils of the anode, this is a 0.25% effect, a 0.9° effect, i.e. a $\pm$10 m/sec effect. This is not a negligible effect, in fact it is equal to the maximum error, but it is a systematic effect which can be corrected in ground processing.
2. For 15 and 20 mils spot sizes there is no measurable aliasing with very little random error. The azimuthal measurements have a spreading of well under 0.05°. Once the systematic distortion mentioned above is removed, the radial measurements have a spreading of well under 0.1 mil, i.e. 0.02°. Indeed these residual fluctuations could be numerical artifacts.
3. For a 10 mil spot radius, aliasing is visible. The worst-case azimuthal aliasing is $\pm$0.5° and occurs at an azimuth of 180°. Small fluctuations in total charge are observed, only 0.1% but indicating that a measurable fraction of the charge cloud is being lost. The period is equal to the wedge-wedge spacing, and since thermal spreading will smear an incident spot over several wedge pairs, this should contribute to a random spreading rather than any systematic effects.
4. The anode region where accurate results could be obtained depended on spot size and was worst for the 20 mil spot. For an anode going from 260 to 530 mils, the region where the response was extremely linear was limited to 310 to 470 mils. Outside of this region, systematic distortions in both elevation and azimuth were observed.

It should be noted that the model assumes that wedge boundaries are very accurately known. Real-world fabrication processes can cause some distortion in the wedge boundaries, that is likely to cause broadening beyond that computed here. However, we are optimistic that by making use of current fabrication techniques such deleterious edge effects can be virtually eliminated, and an anode with the potential of making very accurate measurements indeed, can be realized

5.5 Anode Optimization

We can now consider the question of how we optimize the anode. To begin with, this analysis indicates that the current anode design will do fine. It will deliver the necessary resolution and can certainly be fabricated. Some noteworthy observations are as follows:

(i) we cannot make the wedge pairs any larger than they now are, or aliasing will become significant.

(ii) we don't want to make any feature sizes or spacings smaller than we currently have, or fabrication will either become more difficult due to increased tolerances or will lead to more fluctuations due to changing wedge sizes.

(iii) it has been proposed that the single azimuthal cycle pattern be replaced with two or more cycles. Adding more cycles adds considerably to circuit complexity. In fact, it is not clear that we can put two or four times the analog electronics on the board. Further, this analysis shows that this is not required to obtain the needed resolution, as a single cycle does just fine.

(iv) it has been proposed that interstitial elements be inserted between the wedges. If the 1-mil feature size is kept, it is clear that these additional elements would increase the radial offset between wedges, and consequently increases the radial aliasing with azimuth for all events. This will also increase the dead area fraction, thus increasing azimuthal aliasing with radius for the smaller events. This analysis shows that it is not required.

One change that is reasonable to make is to increase the width of the "tail", from 1 mil to say 1.5 or 2 mils. This will have essentially no impact on the elevation measurement, which is determined from the number of anode pairs. For the azimuthal measurement, the radial offset between the centers increases somewhat, thereby increasing the radial aliasing with azimuth. The noise σ_A will be unchanged. However, the range of A will, in general, decrease. How much it decreases with tail width is difficult to compute, but it clearly does decrease (consider the limit of the tail equal to the head). The signal to noise ratio thus decreases - we lose the ability to accurately measure azimuth. The only reason to do this would be if fabrication tolerances make it uncertain that we will get accurate, 1 mil tails.

5.6 Electronic Noise

From the sketch of the *Backgammon* anode concept shown in Figure 6, it can be seen that an incident charge Q is deposited over a small region at a location (illustrated by the shaded circle). The charge is divided between the four charge amps, with the division depending on location. The azimuthal charge division is based on the aspect ratio of the anode, while the elevation charge division is based on the capacitive divider chain. The location of the centroid of a charge cloud is determined from the four measured charges V_A through V_D, in the two orthogonal axes, as:

$$Azimuth = \frac{(V_A + V_B) - (V_C + V_D)}{V_A + V_B + V_C + V_D} \qquad Elevation = \frac{(V_A + V_D) - (V_B + V_C)}{V_A + V_B + V_C + V_D}$$

There are many variants on this basic concept. As previously mentioned, in DIDM, the anode is cylindrical and thus the rectangular geometry shown in Figure 6 maps into a polar geometry. The anodes can be "asymmetric" as indicated, or can they can be symmetric. The Azimuth and Elevation expressions can be differential, as shown above, or single-ended. All these variants are conceptually similar. It can be argued that what is presented is the best in terms of precision and accuracy.

There will be some inevitable fluctuations in the measured charges V_A through V_D, due to electronic noise and to quantum fluctuations. An estimate was made of the magnitude of these fluctuations, to see if they will degrade image resolution. Both elevation and azimuth are determined by expressions of the form:

$$A = \frac{P - M}{P + M}$$

where: P and M are the sum of two preamplifier outputs, i.e. P=V_A+V_B or V_A+V_D, depending on the axis. With the currently planned15 wedge pairs with an aspect ratio of 15:1 (each wedge has a "tail" 1/15 the "head), P and M each cover the range of about 0.1 to 0.9 times the total charge, so A ranges from -0.8 to +0.8. The quantity "A" shown here must be scaled appropriately to give the actual range, i.e. 0° to 35° or 0° to 360°.

To get the uncertainty in A requires a bit of derivation[8]. In general, if we have A=f(P,M) where P and M have statistically independent errors σ_P^2 and σ_M^2. Then:

$$\sigma_A^2 = \left(\frac{\partial f}{\partial P}\right)^2 \sigma_P^2 + \left(\frac{\partial f}{\partial M}\right)^2 \sigma_M^2$$

We have

$$f = \frac{P - M}{P + M}$$

$$\frac{\partial f}{\partial P} = \frac{1}{P+M} - \frac{P-M}{(P+M)^2} = \frac{(P+M)-(P-M)}{(P+M)^2} = \frac{-2M}{(P+M)^2}$$

$$\frac{\partial f}{\partial M} = \frac{-1}{P+M} - \frac{P-M}{(P+M)^2} = \frac{-(P+M)-(P-M)}{(P+M)^2} = \frac{-2P}{(P+M)^2}$$

$$Var\left(\frac{P-M}{P+M}\right) = \left(\frac{-2M}{(P+M)^2}\right)^2 Var(P) + \left(\frac{-2P}{(P+M)^2}\right)^2 Var(M)$$

Assuming that $\sigma_P^2=\sigma_M^2$,

$$\sigma_A^2 = \left[\frac{4\left(P^2 + M^2\right)}{(P+M)^4}\right]\sigma_P^2$$

Assume now that our minimum gain is $1x10^6$. We can consider two limiting cases, where P=M=0.5x106 (near the middle) and where $P=0.1x10^6$ and $M=0.9x10^6$ (or vice-versa, near either end). It is reasonable to assume that σ_P=3,000 electrons rms or less - this is a reasonable number for the electronic noise. Then:

Middle:

$$\sigma_A^2 = \left[\frac{4\left(\left(0.5\times10^6\right)^2 + \left(0.5\times10^6\right)^2\right)}{\left(1\times10^6\right)^4}\right]\left(3\times10^3\right)^2 = \frac{\left(2\times10^{12}\right)\left(9\times10^6\right)}{1\times10^{24}} = 18\times10^{-6}$$

$$\sigma_A = 4\times10^{-3}$$

Ends:

$$\sigma_A^2 = \left[\frac{4\left(\left(0.1\times10^6\right)^2 + \left(0.9\times10^6\right)^2\right)}{\left(1\times10^6\right)^4}\right]\left(3\times10^3\right)^2 = \frac{\left(3\times10^{12}\right)\left(9\times10^6\right)}{1\times10^{24}} = 27\times10^{-6}$$

$$\sigma_A = 5\times10^{-3}$$

Since A covers a range of -0.8 to +0.8, at all locations, the electronic noise causes <0.3% measurement uncertainty. This is assuming an electronic noise of 3,000 electrons rms, which is probably conservative - the real noise is likely to be less. This also assumes a gain of $1x10^6$. The

resolution goes inversely with gain, so increasing gain will help. The gain could be lowered somewhat before electronic noise would start to become a problem.

We have previously discussed a "single-ended" measurement, using P alone in the numerator instead of P-M. The differential measurement doubles the range of A, i.e. doubles the signal. For the noise, the (P^2+M^2) in the numerator for the differential measurement becomes P^2 alone for the single-ended measurement. Basically, with a differential measurement the noise increases by about $\sqrt{2}$ while the signal doubles, so the signal to noise ratio increases by $\sqrt{2}$. The actual situation is a little more complicated, since for the single-ended measurement the noise is more dependent on position.

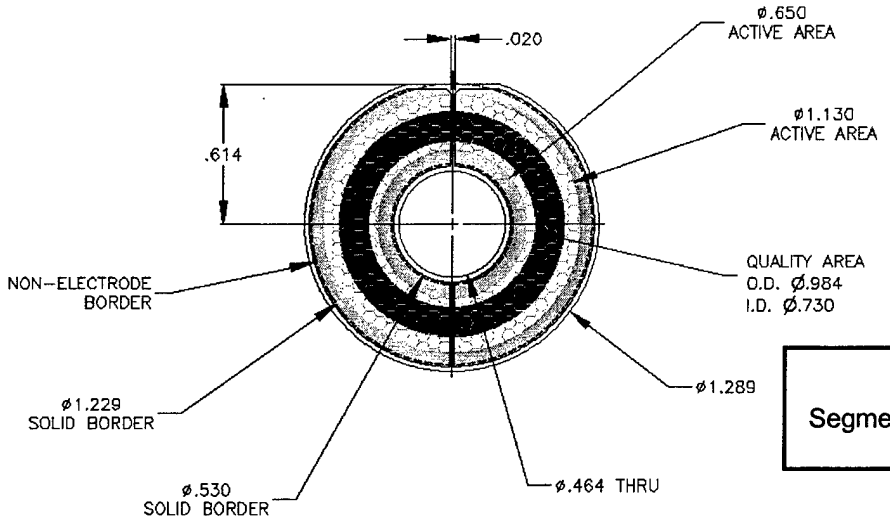

Figure 8:
Segmented Micro-Channel Plate

5.7 MCP Design

Another of the new and innovative features in the proposed DIDM-3 design, is the use of a novel design and enhanced performance type micro-channel plates (MCPs). MCPs are a key feature in the detection of incident ions. They are particle multipliers. Each incident ion strike on the MCP surface results in the generation of more than 10^5 electrons at the exit side of the device. It is this cloud of electrons, collected by the position sensitive anode, which permits the detection of single ions by the instrument.

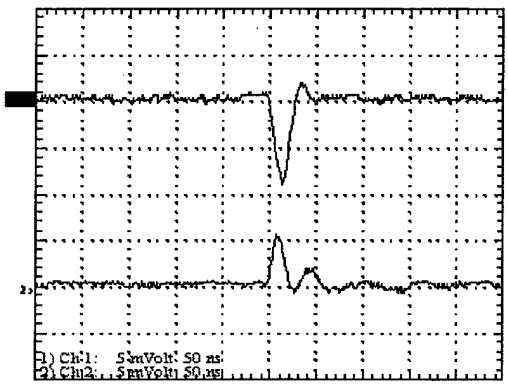

Figure 9: MCP-Analog Design
Verification Results

In the DIDM-3 design, in addition to the basic detect function, the custom MCPs (see Figure 8 for details) are of an enhanced performance type that is optimized for high count rates. The units are also segmented into two separate halves, in order to facilitate absolute position determination on the new *Backgammon* Anode. The anode pattern is entirely symmetrical in design and it is necessary to know which half of the MCP fired, in order to determine the exact incident position for an ion. The MCP generates a return current in its contact rings, through which the -2kV necessary for the device to operate is applied, and the occurrence of this current in either half of the MCP is used as evidence of a detect event in that particular half. Furthermore, the contact ring current is also used as a start pulse for event detect timing in the signal processing associated with each event.

It was necessary to verify that a good basis for these key features of the instrument's analog design does indeed exist. In fact, it was first necessary to establish that it can be done. Specifically, the MCP return current had to be examined to determine if it was of sufficient amplitude, as well as, fast and quiet enough for use in this application. If it was not, techniques had to be devised to make it possible. By using the test facilities (vacuum chamber and sources) at Amptek, and an assembly of DIDM-2 components, which although different from that to be used for DIDM-3, was sufficiently similar for the exercise to be entirely meaningful, it was clearly established that the implementation of this aspect of the DIDM-3 design would not be a problem. Figure 9 shows plots of the anode signal response for an incident ion event (top trace) and the MCP return current signal (bottom trace) on a common time base. Although some effort was required to finally obtain this very clean output for the MCP signal, it does show that it can be done. Note also the direct correlation in timing for the start of the two signals, which clearly establishes that the return current signal can indeed be used as a valid start pulse in the processing of anode signals.

5.8 Digital Pulse Processor (DPP)

One of the most challenging requirement for the DIDM-3 instrument is that it shall *have an overall count rate capability of no less than 1 x 10^6/sec.* The implementation of this capability requires an entirely new approach to signal processing within the instrument, since the existing technique is fundamentally incapable of realizing such a throughput; especially with the added constraint of less than 5 Watts average power consumption. The DIDM-2 signal processing design is of limited utility when very fast data acquisition times are necessary, since it is only capable of a 40μs analog-to-digital convert time in the processing electronics. This could be reduced somewhat with the use of faster electronic components, but only at the price of increased power consumption, and a possibly compromised space-flight capable instrument, since there is no guaranty that the faster parts will be available in a space-rated grade. Also, the signal processing design for the anode signals seriously limit the rate at which the instrument could operate.

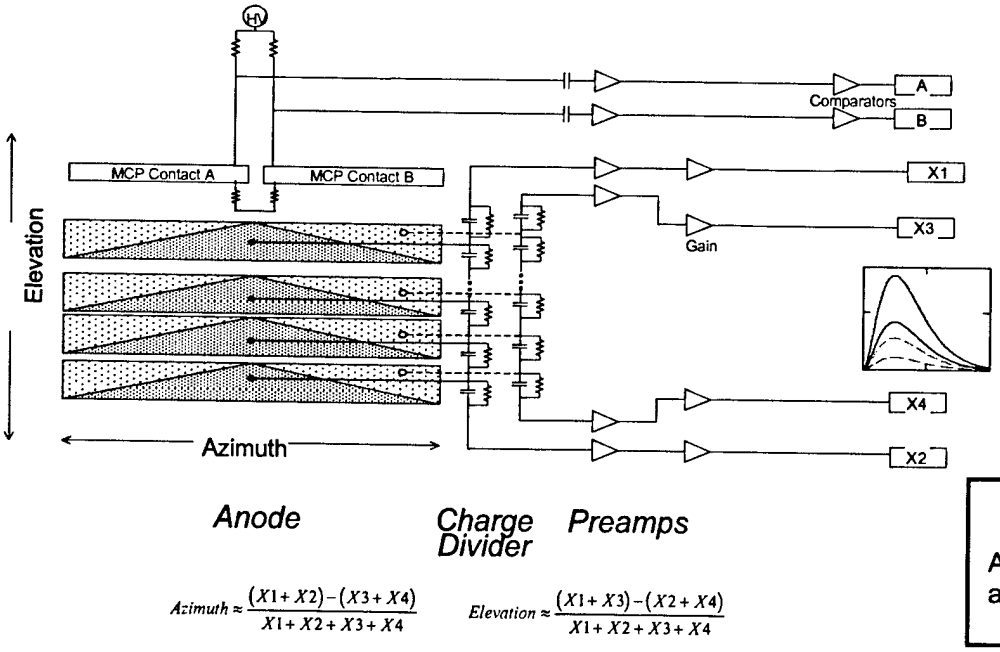

Figure 10:
Anode Position Determination Signals Schematic

The signal processing technique for position determination is ultimately limited by pulse pile-up and/or baseline restoration concerns, to less than an order of magnitude improvement over the DIDM-2 capability. In the plethora of novel ideas being proposed for DIDM-3, another of the new and innovative design features is the use of a Digital Pulse Processor (DPP) technique to comfortably

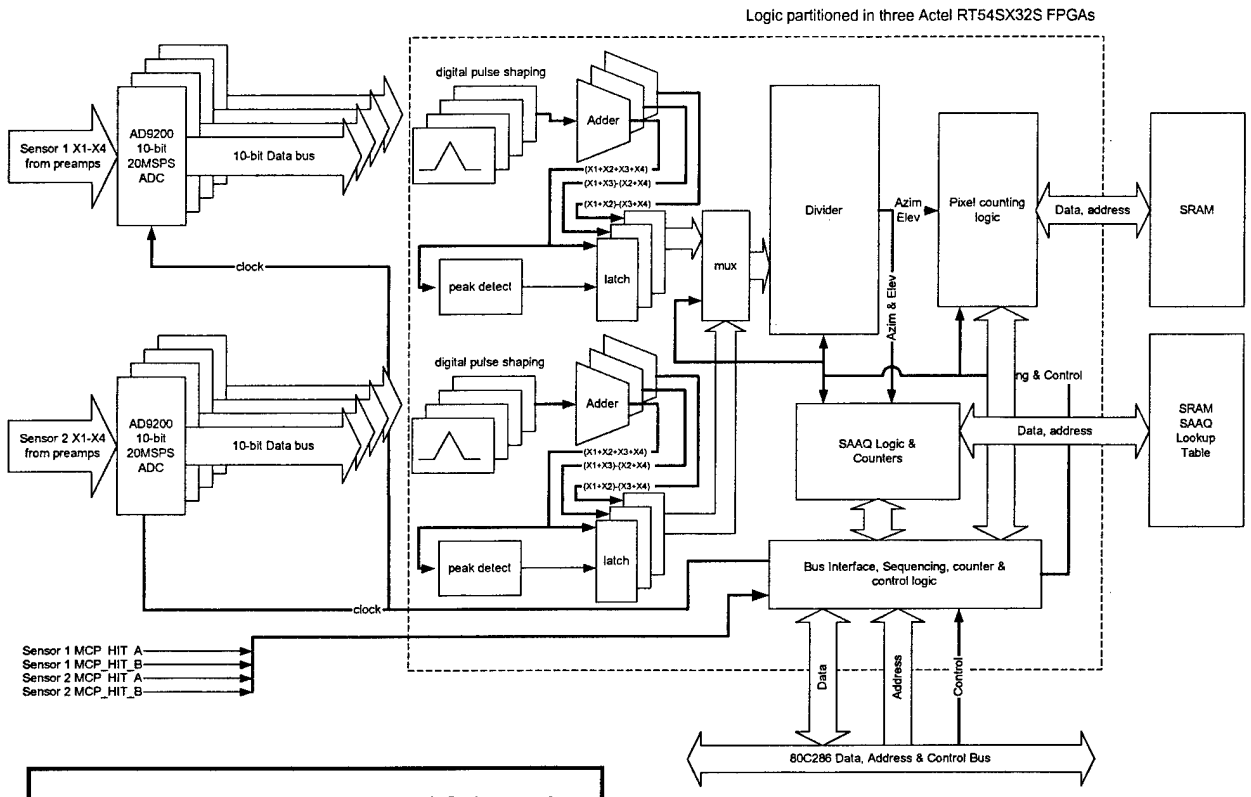

Figure 11: DPP Board Functional Schematic

realize an overall count rate capability of greater than 1 x 10^6/sec. With this implementation, Amptek, Inc. will be bringing to spacecraft diagnostic instrument design, state-of-the-art techniques and technologies that the company is currently developing for its commercial x-ray and γ-ray detector instruments.

There are two major aspects to the proposed signal processing design. The first is that it is an all-digital design, which means it is: (a) fast; and that (b) all of the traditional analog functionality of pulse shaping, differentiation, peak hold, baseline restoration and pile-up reject, can either be implemented digitally, or are not required. This not only reduces considerably the amount of power needed to implement the required functions, but also makes available a substantial amount of circuit board space, for hardware implementation of other utilities such as interfacing to peripherals, and device control programming. The second aspect to the design consequently, is that it is very compact in size and in power consumption. It is anticipated that the DIDM-3 stack will be at least one card less than was necessary for the previous DIDM. These improvements are made possible by the recent availability of space-rated Field Programmable Gate Arrays (FPGA), which are integrated circuits with a very large number of logic gates, that can be used to implement functionalities that were previously done with discrete electronic components.

The specifics of the proposed DPP design, which is shown in block diagram form in Figure 11, can be described as follows: the pre-amp signals coming off the anode (illustrated in Figure 10) are digitized by a fast (20 MHz rate) analog-to-digital converter (ADC), and the 10-bit output from each of the four individual sensor ADCs are fed directly into a dedicated FPGA module for each sensor. All subsequent processing to determine the incident azimuth and elevation coordinates will then take place within the FPGA modules. The data streams are first shaped and added to generate two numerators and a denominator. The adder outputs subsequently go into a divider, which determines azimuth and elevation coordinates directly. The coordinate information is then shifted to both a pixel counting 16 x 32 array and Synthetic Adaptive Aperture Quadrature (SAAQ) counting

logic blocks, which will also be within the same FPGA if there is room, or in a third FPGA module if necessary. It is also proposed that the additional functionality of generating timing signals from the MCP hit signals, handling data address and control bus interfacing with the microprocessor, as well as, handling logic blocks data and address interfacing with the SRAMs, also be designed into the FPGAs. With this substantial amount of functionality implemented in the FPGA modules within the DPP, and with it all running at a rate consistent with the 20 MHz ADC sample rate, it is expected that the DIDM-3 instrument will easily realize an overall count rate capability greater than 1 x 10^6/sec.

Details regarding the overall performance of Digital Pulse Processors are well known and recorded in the published literature[9]. A substantial basis for the expected signal processing performance can be determined from this source. However, in order to get a handle on the *front-end* electronics performance of the instrument design, a prototype DPP was fabricated and tested in-line with a *Backgammon* anode simulator. The results thus far are extremely encouraging. To illustrate,

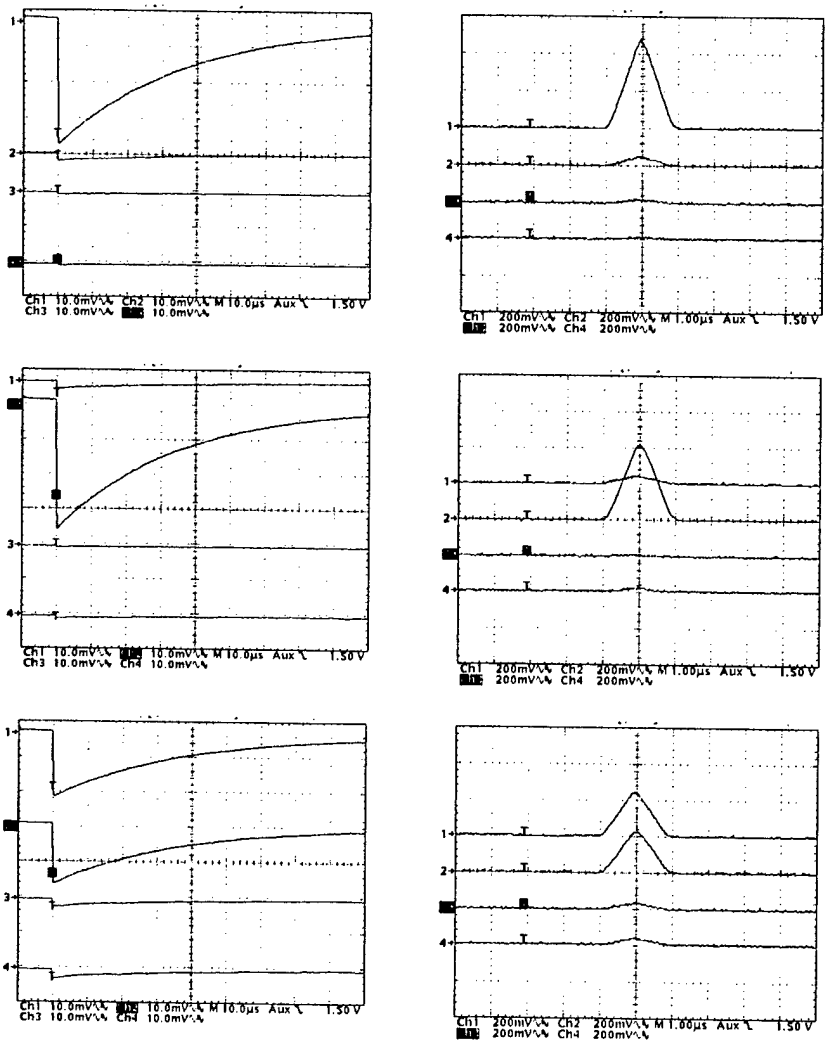

Figure 12:
Benchtop Charge PreAmp Outputs (left) and Corresponding DPP Analog Outputs (right).

three pairs of plots are shown in Figure 12, each of which has four traces representing the four signal paths from the *Backgammon* anode simulator. Each pair of plots show the charge preamp output (on left), and the shaped DPP analog output (on the right) for a stimulus at a different location on the anode simulator. It is seen that charge amplifier outputs are stable and very clean (no distortion), in response to an anode stimulus of approximately 10^7 electrons (typical for MCP output). The corresponding DPP analog response is shown in the plots on the right. Note that incident position on the anode is determined from the shaped DPP signals and much of the design battle to date, had to do

with realizing signals with so little distortion and timing skew, as to make the final DPP output satisfactory from a measurement accuracy and precision standpoint.

Having achieved this much, it is reasonable to conclude that proof of the soundness of the detection scheme for the *Backgammon* anode (*front-end* design) has been established. Implementing the translational algorithms that convert DPP signals into incident position is a relatively straightforward matter. It is expected that the DPP will incorporate three of the RT54SX325-CQ208 Actel FPGAs, but the detailed design is not yet completed and this could change. The FPGAs are modular devices and both the DPP design, as well as the Actel design tools are readily scaleable, so that additional units can and will be utilized if necessary, in order to accomplished the desired performance objectives.

5.9 Sensor Design and Assembly

The true driver behind the decision to integrate the sensor assembly into the electronics module was the need to reduce the complexity of the assembly. Putting together the previous sensor assemblies was a truly intricate, time consuming, difficult and oftentimes frustrating endeavor. There was a crying need for a simpler sensor design and correspondingly, an easier assembly process. With the proposed design, it remains the case that there are many different parts in the assembly, but the process of putting it all together is relatively straightforward and greatly simplified. An illustration of the entire assembly is shown in Figure 14(a). The design is a modular one, with separate sections on either side of the anode board. Both sections can be individually assembled, and then mated with the anode board to complete the assembly. Solid model views of the two halves are shown in Figure 14(b) for the aperture assembly module, and in Figure 14(c) for the backplane assembly module.

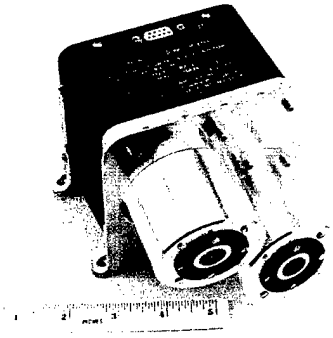

(a)

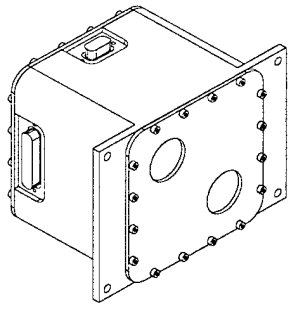

(b)

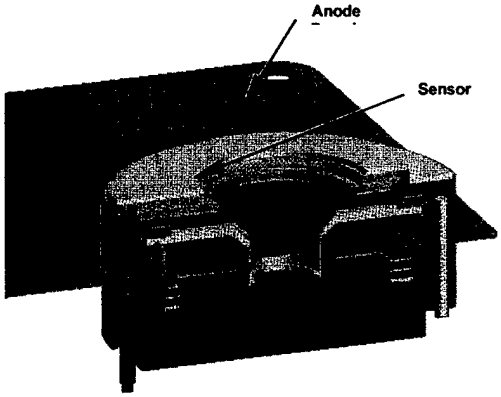

(c)

Figure 13: (a) DIDM-2 Instrument
(b) Proposed DIDM-3
(c) New Sensor Assembly Integration Method

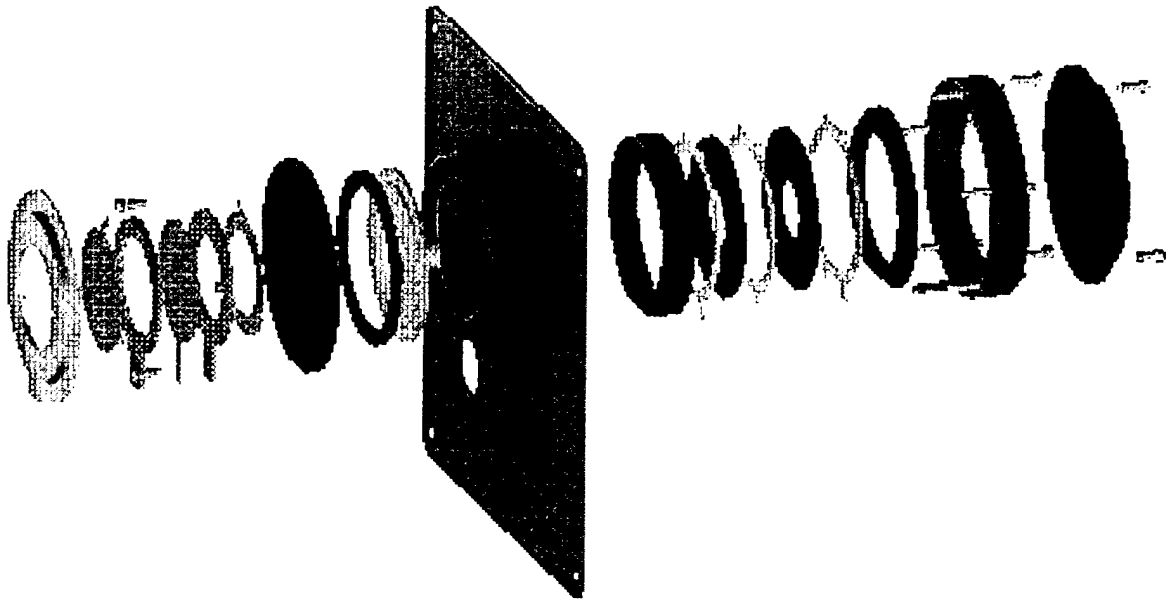

(a)

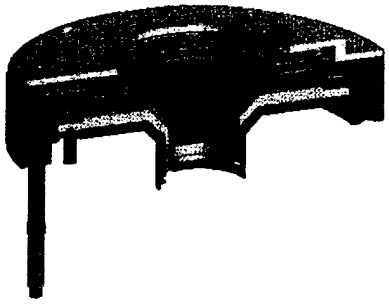

(b)

(c)

Figure 14: (a) DIDM-3 Sensor Assembly
(b) Aperture Assembly Module
(c) Backplane Assembly Module

5.10 Anticipated Instrument Performance

The DIDM-3 instrument operates on the same so-called *charge sharing* operational principle as DIDM-2. The term refers to the means by which incident position is determined on the position-sensitive detecting anode. In this regard, the *Backgammon* anode scheme is identical to that previously used for the *wedge and strip* anode, in terms of functionality, as well as in the accuracy and resolution of the measurements. This means that anode signals can be binned into the desired number of discrete voltages, consistent with the required level of accuracy and speed of operation. The possibility of high measurement accuracy inherent to the charge sharing technique is consequently in the instrument design. Extensive computer simulation modeling here at Amptek has shown that better than 1% measurement accuracy achievable in the determination of both azimuth and elevation angles.

As has been previously mentioned, one major change for DIDM-3 is in instrument data throughput. The data acquisition rate is to be increased from the DIDM-2 maximum rate count rate of 25kHz in the drift-meter operating mode, to greater than 100kHz. The goal is to achieve 10^6Hz. In this regard, the instrument will have considerably enhanced data processing capability, in order to continue to make the precise measurements required.

6. HARDWARE DESIGN

6.1 Outline

The preliminary design for the DIDM-3 enclosure is shown in Figure 15. It is a single small enclosure, with two interface connectors for power (J1) and telemetry (J2). The overall dimensions are 15 x 11 x 0.95 cm^3. The final weight is expected to be much less than the 2.2kg for DIDM-2, a savings of greater than ½ lb will be realized by the elimination of the externally mounted sensor assemblies. The potential for additional weight savings also exist in the 0.190" wall thickness, which

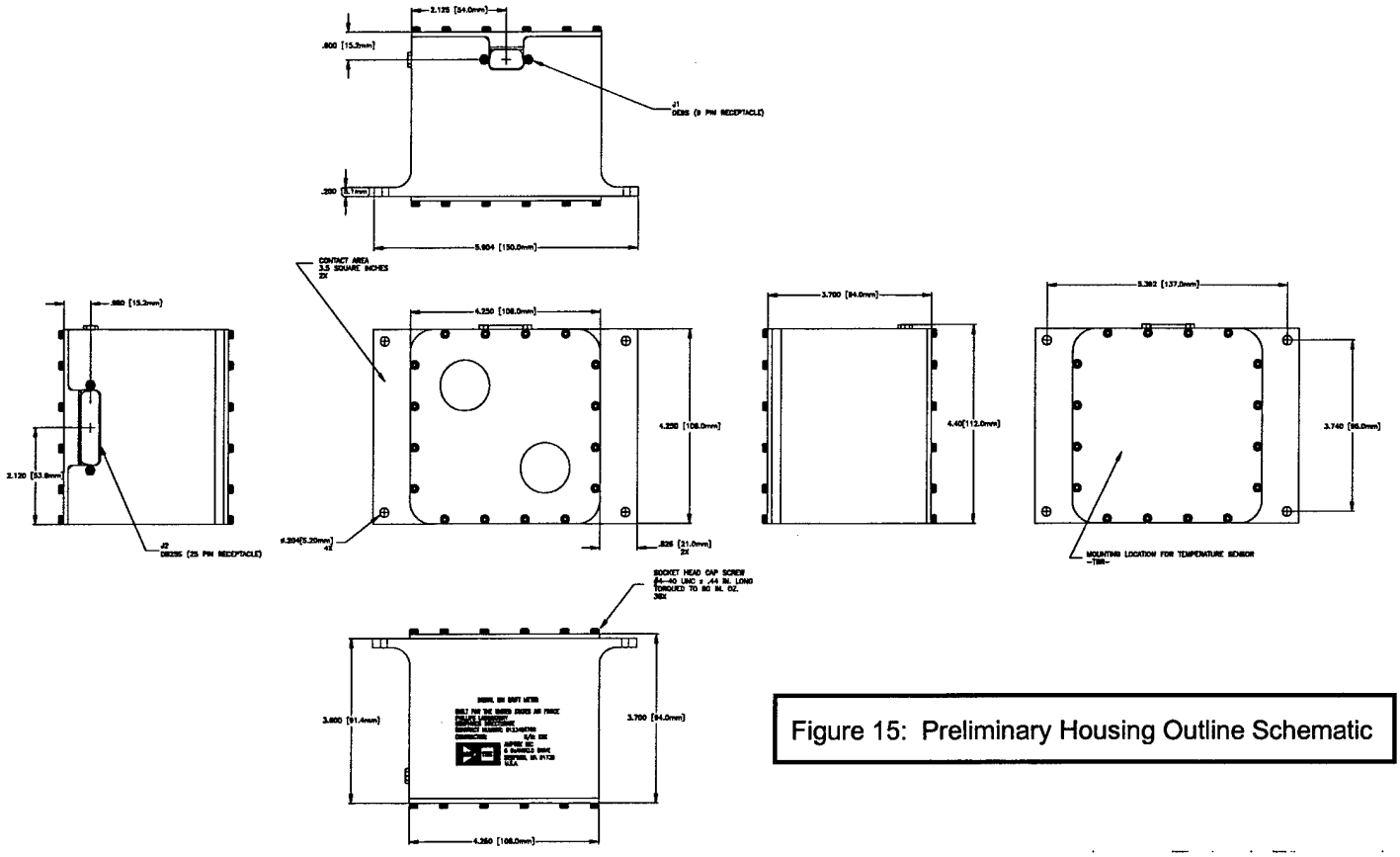

Figure 15: Preliminary Housing Outline Schematic

can be thinned for the C/NOFS mission, since shielding against radiation dose is not a mission concern. This was not the case for the DIDM-2 instrument and hence the enhanced wall thickness was introduced for total dose protection. In principal, the wall thickness should be limited only by structural integrity concerns, and in this regard it could be reduced to less than 0.100".

The housing design awaits decisions on the specifics of the instrument's mounting arrangement on the spacecraft, before it can be finalized. Still to be decided for example, are: (i) the required mounting flange location. It is currently shown on the front face of the instrument, but it can be moved to the rear face, or points in between, as necessary. (ii) the question of whether the screws that hold the front face to the enclosure's sidewalls can be recessed, was raised in a systems review meeting. Should the screw heads on the face prove to be an obstacle, the design can easily be changed to remove them. (iii) as previously mentioned, the wall thickness can be reduced appreciably,

especially if it would be beneficial to do so from a weight reduction standpoint. This decision hinges on a good assessment of the weight balance on the spacecraft. Given that the DIDM instrument is ultimately capable of making very precise $\overline{E}$ field measurements, the considerable difference in size between the instrument's housing and the typically long booms that are characteristic of the traditional $\overline{E}$ field measurement instruments, DIDM-3 should make a very attractive candidate for these types of *in-situ* investigations.

6.2 Board Stack

The instrument is made-up of five 4" x 4" printed circuit board cards, surrounded by the enclosure shown in Figure 8. This stacked printed circuit board design (see Figure 16) of the DIDM electronics module is a good one and will also be retained for the DIDM-3 instrument. Each functional element that make up the electronic module is on a separate card, and these in turn, are connected together via an array of mating pins and sockets (only one shown for clarity), that are placed along a common side on each board. Four rods run through the corner of each card and a solid aluminum spacer on each of these rods separates the boards, and further adds to the mechanical integrity of the assembly. The top card is the Sensor-Preamp (SPRE) board. It is followed in turn, by the Digital Pulse Processor (DPP), Central Processing Unit (CPU), Telemetry Interface (INT) and Power Supply (PWR) cards. The names describe fairly well, the functionality associated with each card. The DPP card is the significantly new entry for DIDM-3. Its principal function is to process the incident event signals from the anode and generate the incident angle coordinates. The means by which it achieves this result is one of the innovative features of the DIDM-3 design. Additional information on DPP functionality will be provided in subsequent

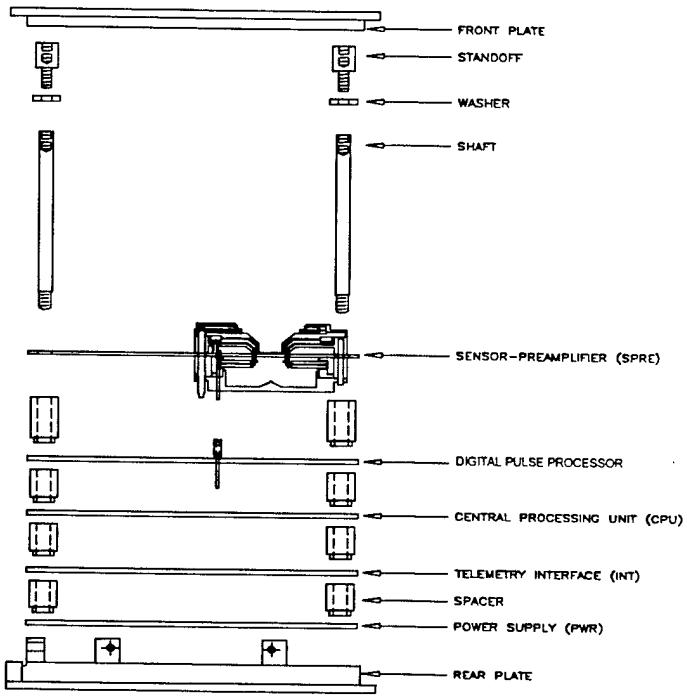

Figure 16: DIDM-3 Board Stack

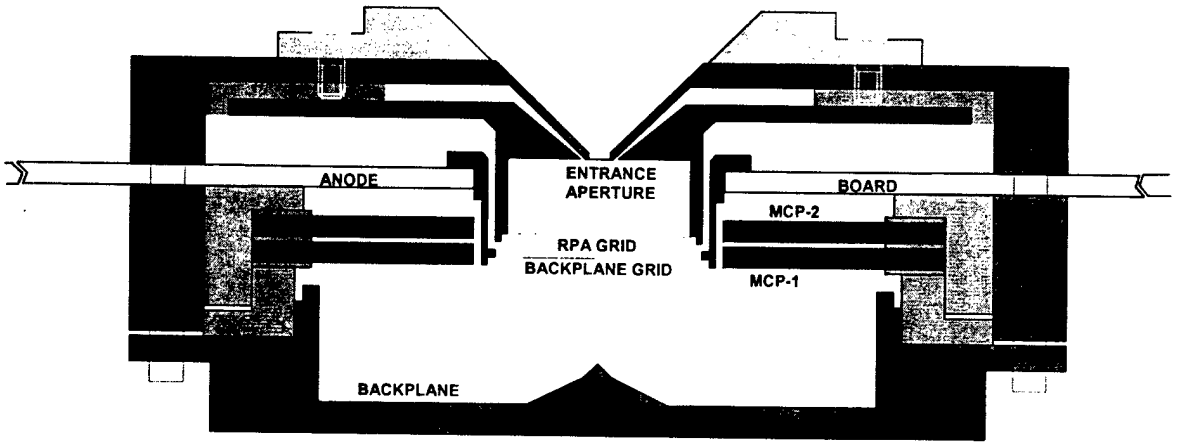

Figure 17: Cross-Section View of DIDM-3 Sensor

material. As in the DIDM-2 design, it is anticipated that the second board up from the rear plate will be the telemetry interface to the spacecraft. The C/NOFS requirement is for this interface to be MIL-STD-1553 compliant. Amptek, Inc. not only has the experience of implementing such an interface before (it was communications interface for the DIDM-1 instrument), but also has in its possession residual hardware and software tools from that effort, to aid in implementing the same for DIDM-3.

The DIDM-2 instrument was flown with a Planar Langmuir Probe (PLP) to acquire temporal spacecraft potential information and optimize the acquisition of drift meter data. There was therefore a dedicated PLP interface board in the stack for this purpose. The DIDM-3 design requirements state that it is necessary for DIDM-3 to *respond to spacecraft potential data input from another instrument,* and it is proposed that this data transfer be done via the MIL-STD-1553 interface. In this manner, DIDM-3 will inherently be capable of satisfying the requirement.

6.3 Sensor Assembly

In an effort to get a handle on and optimize the impact of the design changes on sensor performance, a fair amount of time was spent installing and coming up to speed on the SIMION electrostatic ion optics simulation tool. The version of the code which runs on a PC was developed at the Idaho National Engineering and Environmental Laboratory, and it has evolved as a distinctly separate effort from the original (mainframe) development in Australia. The latest version was procured from the USDE Energy Science & Technology Software Center for a nominal sum. After installing the software and coming to some understanding of its workings, the next step was to generate the essential mechanical elements of the sensor within the program, so that basic design functionality could first be established. Subsequently, elements within the assembly could then be changed and the impact on performance determined.

A large degree of success with the design verification effort was achieved when the results shown in Figure 18 were achieved. The plot shows the trajectories for an incident fan of ions (black lines) through the entrance aperture, and terminating on the surface of the front MCP surface (see Figure 17 for feature designations). The other lines (shown in color red) represent the potential contours within the sensor assembly. Note that the sensor assembly is cylindrically symmetric and only one half of the entire response is shown. A key aspect of this effort is to linearize as much as possible, the extent of the ion impacts on the MCP. It can clearly be seen in Figure 18 for example, that trajectories are bunched (to some extent) at both ends of their trajectory range. Such behavior results in a non-linear response in these areas and effectively limits the usefulness of the instrument. The reason for this occurrence is the influence of the potential contour lines and correspondingly the electrostatic field lines (which are perpendicular to the potential contour everywhere), which the ions follow. In areas where the potential is high (tightly concentrated contour lines) the impact on ion trajectories is to provide a substantial kick that excludes them from such areas. This is undesirable and it is clear that removing such features from likely ion pathways would be beneficial.

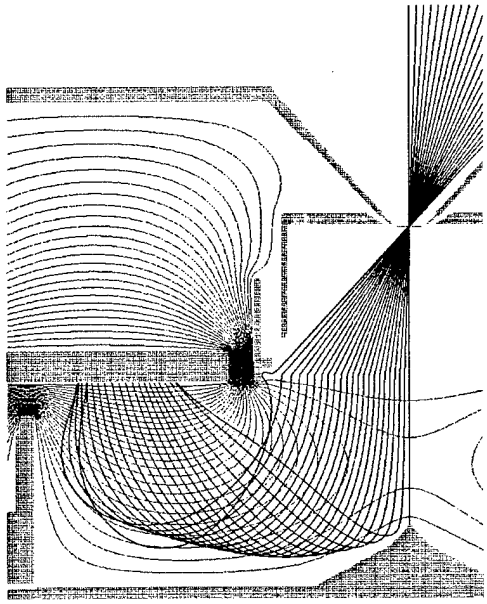

Figure 18: Simulated Ion Trajectories Inside DIDM Sensor Assembly From SIMION

6.4 Sensor Design and Particle Gating

An integral feature of previous DIDM instruments is a particle gate. One important issue that was addressed and resolved in the latest instrument design, is the question of whether or not particle gating is really necessary for DIDM-3 as well. The DIDM-2 gate is a fine wire mesh in front of the instrument's aperture, which is held at a high potential (≈ 28V) relative to that of the incident ions (<1.0eV in energy), to 'screen out' incident ions when necessary. It is rapidly collapsed to 0V to allow them in. Implementing the gate in the sensor assembly not only adds to the challenge and complication of the mechanical design, but also complicates the electrical design. This is due to the fact that, ideally, the voltage transitions on the gate should occur instantaneously, i.e. in zero time. Of course, there are practical considerations which limit the rate at which both the gate-on and gate-off transitions can occur, and not the least of these are the instrument's size and power constraints. In addition, such rapid electrical transitions easily couples into the event detect or other instrument signal processing circuitry and corrupt their true amplitude and/or timing. The prevention of this kind of interference from happening is generally not a simple and easy thing to do and not having to deal with the difficulty in the first place is obviously the preferred solution. Furthermore, legitimate questions have been raised about the impact of the gate on both trajectory and energy of incident particles, and the corresponding influence on the instrument's drift velocity determination. Speculation has been directed in particular, towards the issue of whether or not ions which would otherwise not be incident in the instrument, are trajectory impacted by the operation of the gate, such that they make it to the aperture and counted by DIDM, or vice versa. Clearly, not having a gate would immediately dispel questions of this kind

The analysis shows that a DIDM-3 design can be successfully implemented without the use of a gate. The performance summary for two different aperture sizes are shown in Figures 19(a) and 19(b). On both plots, the environmental parameter space to be measured by the instrument on the C/NOFS mission is shown bounded by the inner (solid line) rectangle. The expected instrument performance range is shown bounded on the left by the vertical line inside this box, and by the sloping line on the right. There are actually two vertical lines inside each box. They represent the performance bounds for different assumptions of the required number of counted ions for the instruments output to be statistically meaningful. The left-most line (lavender color) is the statistical limit for 10k counts (5k acquired at 2Hz rate). The other line (green color) is for a limit of 80k counts (5k acquired at 16Hz rate). It has been determined by AFRL that 5k counts is the minimum number necessary for a meaningful drift velocity determination, so looking at multiples of this number is expedient. There is a factor of x2 uncertainty in the assumptions that underlie the calculations for the lower density bound, which suggests that in Figure 19(a) for example, the limit could very well be near the $1x10^3$ cm^{-3} requirement. The uncertainty in the upper density bound is shown by the hash marks immediately to the right of the sloping line.

One immediate conclusion from the analysis is that the parameter requirements cannot be satisfied with a single aperture size. Performance is clearly better with two different sizes. The results for the 3 mil and 6 mil diameters shown cover a fair fraction of the bounded region, but a more optimum coverage might be obtained with other combinations. There is of course, the practical consideration of obtaining smaller diameter apertures, although various solutions do exist. However, according to the DIDM Principal Investigator at AFRL, there is a 6-mil diameter constraint on the upper most size of the aperture. Apparently it was determined during the extensive characterization tests performed on DIDM-2 that the instrument's RPA capability is compromised for larger sized apertures.

One measure of the dynamic performance of the DIDM-3 design is seen in the 'pile-up limit', which is represented by the dashed line just to the right of the sloping upper bound, in both Figures 19(a) and 19(b). This limit is an indication of how well the instrument works without a gate, and it is seen that it is not the limiting factor on performance. Instead, it is the principal detection element in the instrument, the Micro-Channel Plate, which gives rise to the sloping upper bound. This is a tribute to the analog design and the speed of signal amplifiers in particular. These 0.5μs shaping time devices are among the fastest on the market and are catalog items from Amptek, Inc.

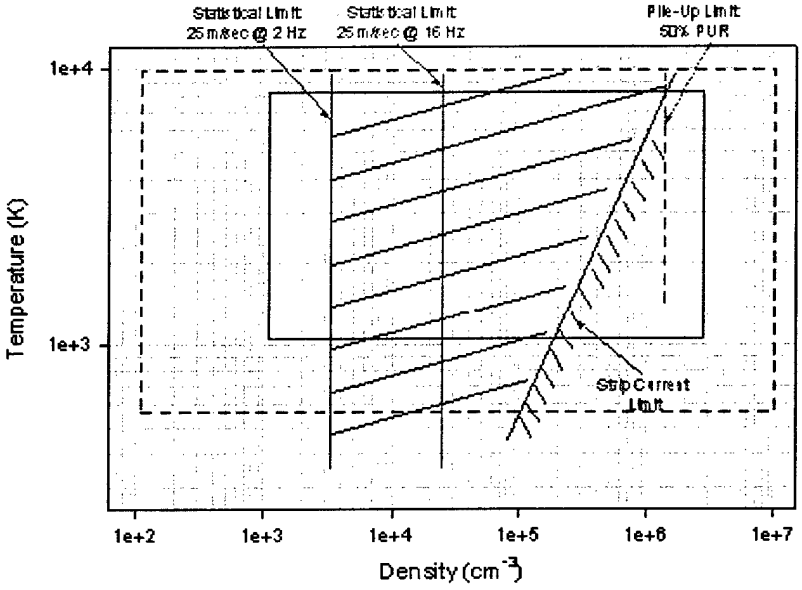

Figure 19(a): No-Gate Performance Summary for 0.006"Aperture.

Other analysis matters that were successfully tackled during the report period, have to do with quantifying the extent of coincident or 'piled-up' events into an un-gated sensor. An assessment of the impact of such events on instrument performance and ultimately on the final drift velocity determination was also made. An in-depth summary of the effort is best presented in another forum, but suffice it to say that while it can be shown there is some impact on the determined ion drift velocity, due to pile-up effects in the sensor, a fair conclusion is that it is of negligible importance.

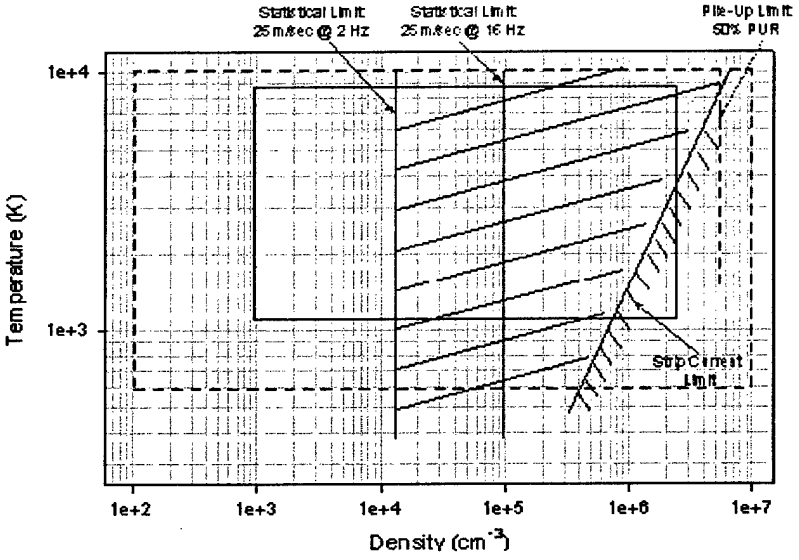

Figure 19(b): No-Gate Performance Summary for 0.003"Aperture.

6.5 Power Supply Design

The power supply design will largely be that of the DIDM-2 instrument. It will be modified to incorporate the ability to step the MCP bias voltage both above and below the nominal -2kV. In this regard, it will borrow aspects of the SSJ5 Electrostatic Analyzer power supply design, which is another of Amptek, Inc's. spaceflight instrument development efforts. The main design features include the following: (i) up to -2500V for MCPs; (ii) high voltage capable of being to be commanded ON/OFF, as well as being stepped ±500V in 50V increments, about the nominal voltage; (iii) 0 to 28V for RPA sweep grid; (iv) sweep voltage to be controlled by the CPU; (v) capable of providing in excess of 6 Watts of power to power MIL-STD-1553B interface. The latter two are inherited features from the previous DIDMs while the other two are unique to DIDM-3.

6.6 Other Sub-System Designs

The MIL-STD-1553B interface in the DIDM-3 instrument will be virtually identical in its hardware implementation, to that used in the DIDM-1 instrument. The other functional module in DIDM-3 is the Central Processing Unit and it will differ little in design from the DIDM-2 version. Functionally of course, there will be differences, as the data processing and telemetry requirements are substantially different. For example, the requirement for uploadable code implies changes to the hardware used in the CPU and I/O circuitry, as well as to the flight software. As has been mentioned previously also, DIDM-2 acquired data at a maximum rate of 25kHz, while the requirement for DIDM-3 is at least 1MHz.

7. SOFTWARE FUNCTIONALITY AND TELEMETRY DESIGN

7.1 Instrument Functionality

In a manner similar to the DIDM-2 design, the DIDM-3 instrument will operate from pre-set instrument configuration sequences enabled via a Configuration Select (Config_Sel) command in a dynamic mode stack. One major utility of this design is that it removes the need for daily configuration command uploads once the instrument is on-orbit, since the configurations may be defined ahead of time, and the execution sequence in the mode stack changed to run them as desired. Additional features of the design are: (i) the instrument will also have fully independent sensor configuration and operations functions; (ii) selectable MCP gain and bias change ranges; (iii) RPA sweep voltage could be scaled for each sensor by a selectable amount; (iv) overall quadrature information returned for pixel array, in addition to adaptive quadrature information. The overall quadrature algorithm operates on the entire pixel map, while the adaptive quadrature algorithm is centered around the centroid (defined as the pixel with highest number of counts per event period); (v) adaptive quadrature boundaries and a bad pixel map are uploadable by command; and finally (vi) the so-called *hybrid* operation mode (i.e. simultaneous RPA and drift meter image operation) is facilitated in the design.

A key feature of the DIDM instrument is that it incorporates a RPA within the sensor assembly, so that energy discrimination of incident ions is possible. The RPA in DIDM-3 is a very capable instrument by itself. Salient features include the following: (i) up to seven RPA sweep profiles, and up to 32 steps per sweep, can be pre-programmed stored for on-orbit selection; (ii) a sweep table allows the period of each step to be selected in the range 25ms to 6.375sec with 25ms resolution; (iii) the step voltage can be selected in the range 0V to 28V with 1/30V resolution; (iv) the selected RPA sweep is automatically repeated after the last step; (v) the RPA sweep voltage for each sensor can be offset by a value uploaded in the Config_Def command; (vi) the sweep on one sensor can be offset in time with respect to the other sensor.

Another heritage feature of DIDM-3 is the so-called *Calibration* mode of operation, which is enabled by provisions in the Diagnostic Select (Diag_Sel) and Config_Sel commands. When executed in the DIDM-2 instrument, the RPA sweep voltage is set to the maximum 28V, and the entire sensor pixel map sampled by moving a variable size pixel stencil through the data in a predefined sequence, stored, and telemetered to the ground over a time period convenient for the download bandwidth. The procedure allows noisy pixels to be identified and removed from the peak search algorithm by ground command. It is a very useful feature and it will be maintained in this instrument as well.

7.2 Commands

In accordance with the C/NOFS spacecraft's MIL-STD-1553 interface protocol, all DIDM-3 commands will be comprised of one 1553 message packet (64 bytes). A preliminary listing of commands is provided in Table 1, which shows the DIDM-2 command listing. Details on a typical

command structure (shown for the Configuration Define [Config_Def] command) are provided in Table 2. There will be a few more commands for DIDM-3. Operational experience with DIDM-2 has shown for example, that the technique used to enable high voltage on the MCPs (a process of first sending the HV-OFF command, followed within a limited period of time by the HV-ON command), is not entirely failsafe, since the HV-OFF command is also used to reset the mode stack. There exists a clear need for a distinct reset mode stack command, and this will be implemented.

Table 2: Preliminary Command Listings

Command	Size (bytes)	Value	Comments
High Voltage ON	**1**	**TBD**	
High Voltage OFF	**1**	**TBD**	
Config. Select	**2**	**variable**	**selects ops mode & duration**
Diagnostic Select	**3**	**variable**	**Pulser Cmd; Quad boundaries; Bad Pixel Map.**
Map Bad Pixel-A	**9**	**variable**	**returns bad pixels for Sensor A**
Map Bad Pixel-B	**9**	**variable**	**returns bad pixels for Sensor B**
Config. Definition	**9**	**variable**	**sets DM and RPA configs; RPA offset; wedge table select.**
Upload Quad Boundary	**9**	**variable**	**Adaptive Quad boundary settings**

Table 3: Command Structure Details

Field No.	Name	Type	Size	Value	Range	Description
1	Command_ID	HEX	8 bits	CONST	7	CONFIG_DEF (Config Define)
2	Parameter 1	HEX	8 bits	VARIABLE	0 - FF	DM A mode
3	Parameter 2	HEX	8 bits	VARIABLE	0 - FF	DM B mode
4	Parameter 3	HEX	8 bits	VARIABLE	0 - FF	RPA A Configuration
5	Parameter 4	HEX	8 bits	VARIABLE	0 - FF	RPA B Configuration
6	Parameter 5	HEX	8 bits	VARIABLE	0 - FF	RPA A offset
7	Parameter 6	HEX	8 bits	VARIABLE	0 - FF	RPA B offset
8	Parameter 7	HEX	8 bits	VARIABLE	0 - FF	Options
9	Parameter 8	HEX	8 bits	VARIABLE	0 - FF	PLP offset

Notes

(i)The RPA Offset voltage values are coded as follows
D7: 0 = absolute; 1 = relative offset
D6: 0 = low range; 1 = high range
D5 - D0: offset count
low range offset = (count*390/4096)-2.47V
high range offset = [(4*count+64)*390/4096]-2.47V
(ii) The PLP Offset voltage values are encoded as follows:
D7: 0 = absolute; 1 = relative offset
D6 - D0: offset count
offset = 39.072mV*count-2.5V
(iii) There are 3 parts to the applied voltage (V_a) for both the RPA and PLP. $V_a = V_s + V_{off} + V_{PLP}$
where V_s = sweep voltage; V_{off} = offset voltage
V_{PLP} = floating potential from PLP.
when D7 = 0, $V_{PLP} = 0$.

DM A/B Mode:

D7 - D5 = 000	no image packets
= 001	1 small stencil packet / DM sample
= 010	1 large stencil packet / 4 DM samples
= 011	1 background packet; sample & hold
= 100	2 background packets; sample & hold
= 101	4 background packets; sample & hold
= 110	8 background packets; sample & hold
= 111	16 background packets; sample & hold
D4 - D3 = XX	Spare
D2 - D0 = 000	0 DM samples/sec
= 001	1 DM sample/sec
= 010	2 DM samples/sec
= 011	4 DM samples/sec
= 100	8 DM samples/sec
= 101	16 DM samples/sec
= 110	Spare
= 111	Spare

RPA A/B Configuration:

D7 - D6 = 00	0 RPA packets in telemetry
= 01	1 RPA packet in telemetry (8 Hz)
= 10	2 RPA packets in telemetry (16 Hz)
= 11	spare
D5 = 0	RPA grounded
= 1	RPA ON
D4 - D3 = 00	No time offset
= 01	1 step time offset
= 10	2 step time offset
= 11	4 step time offset
D2 - D0	RPA sweep number

RPA A/B Voltage Offset:

D7 = 0	Absolute Offset
D7 = 1	Offset Relative to S/C Potential (LP meas.)
D6 = 0	Low Range
D6 = 1	High Range
D5 – 0	RPA Offset Count

Options:

D7 - D5	Define as configuration A through H
D4 - D3 = 00	LP OFF (No electrometer data. Floating Potential data in Status Packet only)
= 01	LP ON/Sweep 1
= 10	LP ON/Sweep 2
= 11	LP ON/Sweep 3
D2 = 1/0	Spare
D1 - D0 = 00	Select wedge table 0 (Default)
= 01	Select wedge table 1 (FWHM)

Additional commanding capability is made necessary with the enhanced MCP high voltage features for the instrument. Recall that in addition to being able to provide a higher (-2500V) MCP voltage, the DIDM-3 high voltage supply will be designed to step in 50V increments, up to ±500V, about the nominal –2000V MCP bias voltage. This versatility will allow ground control to optimize MCP performance throughout the lifetime of the mission via bias control. In the LEO phase of the mission when the MCPs tend to generate excess gain, the bias voltage could be lowered to reduce gain, and towards the EOL phase when conditions generally are reversed, the bias voltage could be raised to increase MCP gain.

7.3 Telemetry Structure

DIDM-3 telemetry will be packetized in 64-byte blocks, in order to conform to the defined C/NOFS data structure. There will be two types of data packets, identified as Type A and Type B. An indication of the proposed contents and size of these packets in given in Table 3. Details on the format are as follows: the most significant bit (D7=1) indicates the packet is a type 'A' packet and contains timecode, status and configuration data. DIDM will only send one Type 'A' packet per second; it will be first packet sent after receipt of the time broadcast. The remaining bits (packet format) indicate the number of DM A, DM B, RPA A, RPA B, packets (where A and B are sensor designations). When D7=0, the packet is a type 'B' packet, and the remaining bits indicate the number

Table 4: Telemetry Data Format

Packet Header

packet counter	3 bytes
packet type*	1 byte
total	4 bytes

Type 'A' packet, format TBD

packet header	4 bytes
sync word	2 bytes
timecode	4 bytes
status	4 bytes
configuration	10 bytes
DM or RPA packet	10 bytes
DM or RPA packet	10 bytes
DM or RPA packet	10 bytes
DM or RPA packet	10 bytes
total	64 bytes

Type 'B' packet, format TBD

packet header	4 bytes
DM or RPA packet	10 bytes
DM or RPA packet	10 bytes
DM or RPA packet	10 bytes
DM or RPA packet	10 bytes
DM or RPA packet	10 bytes
DM or RPA packet	10 bytes
total	64 bytes

Type 'B' packet, format TBD

packet header	4 bytes
image packet	20 bytes
image packet	20 bytes
image packet	20 bytes
total	64 bytes

Table 5: Data in Telemetry Downlink

Minimum

	Cycle 0	Cycle 1	Cycle 2	Cycle 3	Cycle 4	Cycle 5	Cycle 6	Cycle 7	Cycle 8	Cycle 9
	Broadcast time Broadcast sync PLP to DIDM									
DIDM SA1	Type 'A' packet	unused	unused	unused	unused	unused	unused	unused	unused	unused
DIDM SA2	unused	unused	unused	unused	unused	unused	unused	unused	unused	unused
DIDM SA3	unused	unused	unused	unused	unused	unused	unused	unused	unused	unused
DIDM SA4	unused	unused	unused	unused	unused	unused	unused	unused	unused	unused

SGLS uncompressed 512 bps
TDRSS uncompressed 512 bps

• SA 1 is for TDRSS + SGLS. SAs 2-4 are SGLS only.

Maximum

	Cycle 0	Cycle 1	Cycle 2	Cycle 3	Cycle 4	Cycle 5	Cycle 6	Cycle 7	Cycle 8	Cycle 9
	Broadcast time Broadcast sync PLP to DIDM									
DIDM SA1	Type 'A' packet	Type 'B' packet	Type 'B' packet	Type 'B' packet	Type 'B' packet	Type 'B' packet	Type 'B' packet	Type 'B' packet	Type 'B' packet	Type 'B' packet
DIDM SA2	Type 'B' packet	Type 'B' packet	Type 'B' packet	Type 'B' packet	Type 'B' packet	Type 'B' packet	Type 'B' packet	Type 'B' packet	Type 'B' packet	Type 'B' packet
DIDM SA3	Type 'B' packet	Type 'B' packet	Type 'B' packet	Type 'B' packet	Type 'B' packet	Type 'B' packet	Type 'B' packet	Type 'B' packet	Type 'B' packet	Type 'B' packet
DIDM SA4	Type 'B' packet	Type 'B' packet	Type 'B' packet	Type 'B' packet	Type 'B' packet	Type 'B' packet	Type 'B' packet	Type 'B' packet	Type 'B' packet	Type 'B' packet

SGLS uncompressed 20480 bps
TDRSS uncompressed 5120 bps

of DM A, DM B, RPA A, RPA B and image packets. A packet type of 0 (zero) is a zero-filled unused packet.

One of the unique features of the C/NOFS mission is that it will have two different data telemetry paths to the ground. In the initial so-called *Survey Mode* of operation, high bandwidth SGLS transponders will be available exclusively, and it is envisioned that most of the science portion of the mission will be accomplished in this phase. Later on, during the *Forecast Mode* of operation, real-time data will be returned via the relatively low bandwidth TDRSS link. Payloads on this mission must therefore be able to accommodate and operate efficiently, in both modes. As can be seen in Table 4, DIDM-3 output telemetry is structured to accommodate both phases of operation. Shown are the data assignments for each of the instrument's output ports (SA1. . .SA4) on the spacecraft's MIL-STD-1553B interface bus, during each tenth of a second that data will be acquired from the instrument. It is clear then, that DIDM-3 output can be structured to accommodate a minimum 512bps TDRSS data rate, as well as, a SGLS data rate up to 20,480bps. The maximum flexibility to optimize data return, depending on on-orbit opportunities, is consequently provided in the instrument's design.

8. CONCLUSION

From the foregoing material, it is clear that a good deal of the effort required to realize hardware for a DIDM-3 instrument has already been expended. It has been established for example, that a new anode design can be implemented, which from the simulation results, should produce entirely satisfactory results. Also, the new and very much related MCP design has been proven from both manufacturability and analog signal response standpoints. The same can also be said of the digital signal processing design, using the digital pulse processor. The software design for the instrument is well in-hand at this time. The task of writing code has obviously not yet begun, but it is clear what is to be done, and how it is to be accomplished.

A new and substantially enhanced DIDM, capable of making measurements of interest to AFRL therefore awaits a determination to go forward with its development, especially since at the time of writing a decision has been made not to proceed with the effort to put DIDM-3 on the C/NOFS spacecraft. It is hoped that the tremendous capability inherent in this small ($\approx$ 4" cube), light weight (max. 5 lbs), and low power (max. 5 W) instrument, and especially the revolutionary opportunity it offers to make $\overline{E}$ field measurements in space without double probe booms, will not go unrealized.

REFERENCES

1. M. A. Morgan, A. C. Huber, D. J. Sperry, A. Wallace Everest, Scott J. Moran, J. O. McGarity, Marilyn O. Oberhardt, M. Paul Gough and J. A. Pantazis, 1996, Final Report, *Space Systems Environmental Interaction Studies,* Phillips Laboratory Publication No. PL-TR-96-2292, ADA 323403.

2. M. Alvin Morgan, A. C. Huber, D. J. Sperry, A. Wallace Everest, Scott J. Moran, M. Paul Gough and John A. Pantazis, 1998, Scientific Report No. 1, *Space Systems Environmental Interaction Studies,* AFRL Publication No. AFRL-VS-TR-99-1512, ADA 351605.

3. M. Alan Morgan, Alan C. Huber, David J. Sperry, Alan N. Donkin Jr., Scott J. Moran, M. Paul Gough and John A. Pantazis, 1998, Scientific Report No. 2, *Space Systems Environmental Interaction Studies,* AFRL Publication No. AFRL-VS-TR-99-1512, ADA 402285.

4. M. Alan Morgan, Alan C. Huber, David J. Sperry, Alan N. Donkin Jr., Scott J. Moran, Robert H.Redus and John A. Pantazis, 2000, Scientific Report No. 4, *Space Systems Environmental Interaction Studies,* AFRL Publication No. AFRL-VS-TR-2001-1660, ADA 406023.

5. M. Alan Morgan, Alan C. Huber, David J. Sperry, Alan N. Donkin Jr., Scott J. Moran, M. Paul Gough and John A. Pantazis, 1999, Scientific Report No. 3, *Space Systems Environmental Interaction Studies,* AFRL Publication No. AFRL-VS-TR-2001-1610, ADA 405929.

6. F. J. Rich, 1994, Users Guide for the Topside Ionospheric Plasma Monitor (SSIES, SSIES-2 and SSIES-3) on Spacecraft of the Defense Meteorological Satellite Program (DMSP). Volume 1: Technical Description, Phillips Laboratory Publication No. PL-TR-94-2187, *Environmental Research Papers No. 1151.* ADA 315731.

7. D. L. Cooke, L. Wan and F. Rich, 1999, Introducing the Digital Ion Drift Meter, DIDM, *AGU Fall Meeting*, Poster SM12B-01.

8. For example, see Mandel, *The Statistical Analysis of Experimental Data,* Dover Pubs, p 74.

9. For example, see V. T. Jordanov et al, 1994, Digital Techniques for Real-Time Pulse Shaping in Radiation Measurements, Nucl. Instr. And Meth. *Phys Res A353, pgs 261-264.*